

# CO methanation on highly active Ru/TiO<sub>2</sub> catalysts at low CO: H<sub>2</sub> ratios: Mechanism and rate-determining step derived from transient measurements

Ali M. Abdel-Mageed<sup>a,b,\*</sup>, R. Jürgen Behm<sup>a,c,\*</sup>

<sup>a</sup> Institute of Surface Chemistry and Catalysis, Ulm University, D-89069 Ulm, Germany

<sup>b</sup> Leibniz Institute for Catalysis (LIKAT Rostock), D-18059 Rostock, Germany

<sup>c</sup> Institute of Theoretical Chemistry, Ulm University, D-89069 Ulm, Germany

## ARTICLE INFO

### Keywords:

CO methanation  
Reaction mechanism  
Kinetic isotope effect (KIE)  
Rate-determining step  
Ru catalyst

## ABSTRACT

We have systematically investigated mechanistic details of the CO methanation reaction over a supported Ru catalyst in an idealized H<sub>2</sub>-rich reformat gas mixture with low CO:H<sub>2</sub> ratio, employing isotope labelling techniques. From a comprehensive set of transient FTIR spectroscopy measurements, following the buildup / disappearance of different adsorbed species upon exchange of isotope marked reactants during reaction or during desorption, we derive that under these conditions the reaction is dominated by an associative reaction pathway, involving first the formation of adsorbed formyl intermediates, followed by hydrogenation of these intermediates and C-O bond breaking. Formate formation can be excluded. Measurements of kinetic isotope effects (KIEs) revealed a weak secondary inverse KIE with values of  $r_{\text{CH}_4}/r_{\text{CD}_4}$  between 0.6 (175 °C) and 1.0 (230 °C), indicating that at lower temperatures C-H bond formation, most likely HCO<sub>ad</sub> hydrogenation, is rate-determining, while at higher temperatures the reaction is increasingly controlled by C-O bond breaking.

## 1. Introduction

The CO methanation reaction has attracted renewed interest in recent years because of possible applications in power-to-gas concepts, for the conversion of electric power from renewable energy sources into 'green' fuels, or for the catalytic purification of H<sub>2</sub>-rich feed gases for H<sub>2</sub>-operated low-temperature fuel cells containing trace impurities of CO in addition to significant amounts of CO<sub>2</sub> ('selective CO methanation') [1–4]. In these applications, a tightly controlled, very high selectivity of the respective catalysts is of utmost importance, in addition to a high activity and stability. In spite of a large number of studies [1,5–12], the mechanistic understanding of these reactions is still limited and basic aspects of the underlying reaction mechanism are still under discussion. This is particularly true when considering also effects caused by the reaction conditions or by details in the catalyst composition and structure. So far, two basic mechanisms have been suggested. The first one involves the direct dissociation [6,13] or H-assisted dissociation [14] of CO on the metal surface to C<sub>ad</sub> + O<sub>ad</sub> species, followed by a successive reduction to CH<sub>ad</sub>, CH<sub>2,ad</sub>, CH<sub>3,ad</sub> and CH<sub>4,ad</sub> species as well as H<sub>2</sub>O formation. The second reaction route, the associative pathway, proceeds

via the hydrogenation of CO<sub>ad</sub> to form a HCO<sub>ad</sub> intermediate, followed by further hydrogenation and oxygen elimination in one of the subsequent steps. This latter pathway was proposed for different supported metal catalysts such as Rh [15,16], Ni [16,17], and Ru [10,16,18]. Comparable results and proposals were also reported for the first steps of the Fischer-Tropsch reaction on different catalysts and surfaces [19–30]. Iglesia, Mavrikakis, Neurock, and coworkers had underlined that for a number of different metals C-O bond breaking is generally more facile for (partly) hydrogenated CO derivatives ('H-assisted CO activation') than for adsorbed CO itself [25,26,28–30]. This agrees well with our earlier findings for CO methanation on a Ru/γ-Al<sub>2</sub>O<sub>3</sub> catalyst, where under conditions characteristic for the selective CO methanation, i.e., at much lower CO concentrations than in most of the above studies, we could identify adsorbed formyl species as reaction intermediate [18].

In the present contribution we aim at the direct identification of the reaction pathway and reaction intermediates as well as the rate-determining step(s) and their variation with temperature in the CO methanation reaction on a highly active Ru/TiO<sub>2</sub> catalyst at low CO:H<sub>2</sub> ratios, as they are typical for the catalytic removal of CO from H<sub>2</sub>-rich (and CO<sub>2</sub>-rich) gas mixtures ('selective methanation'). Employing

\* Corresponding authors at: Institute of Surface Chemistry and Catalysis, Ulm University, D-89069 Ulm, Germany.

E-mail addresses: [ali.abdelmageed@catalysis.de](mailto:ali.abdelmageed@catalysis.de) (A.M. Abdel-Mageed), [juergen.behm@uni-ulm.de](mailto:juergen.behm@uni-ulm.de) (R.J. Behm).

<https://doi.org/10.1016/j.apcatb.2024.123778>

Received 7 October 2023; Received in revised form 4 January 2024; Accepted 23 January 2024

Available online 26 January 2024

0926-3373/© 2024 The Author(s). Published by Elsevier B.V. This is an open access article under the CC BY license (<http://creativecommons.org/licenses/by/4.0/>).

different transient isotope exchange measurements, isothermal desorption measurements, and measurements of kinetic isotope effects (KIEs), we want to identify reaction intermediates and discriminate them from spectator species by their characteristic shifts in the vibrational bands and the time-dependent formation / decay of the related bands in time-resolved diffuse reflectance FTIR spectroscopy (DRIFTS) measurements to identify adsorbed reaction intermediates and the dominant reaction pathway [18,31,32]. Combining these data provides direct experimental evidence for an associative pathway, via the formation of an adsorbed formyl intermediate, with C-H formation, most likely  $\text{HCO}_{\text{ad}}$  hydrogenation, as rate-determining step. While there are a number of different types of steady-state isotopic transient kinetic analysis (SSITKA) studies on CO methanation and mainly Fischer-Tropsch synthesis on other metal supported catalysts in the literature [14,33–43], including also transient DRIFTS studies [14,34,37,38,42,43], we are not aware of any DRIFTS-based isotope exchange or SSITKA studies on CO methanation on supported Ru catalysts other than our early study on Ru/ $\text{Al}_2\text{O}_3$  [18].

Supported Ru catalysts have been identified as the most active and selective methanation catalysts [5,44]. This is in particular true for Ru catalysts based on reducible oxide supports [1,45–47]. For example, Ru/ $\text{TiO}_2$  catalysts were at least 4–6 times more active than catalysts based on moderately or even non-reducible oxides such as  $\text{Al}_2\text{O}_3$ ,  $\text{ZrO}_2$  or  $\text{SiO}_2$  [1,10,12,48–51]. At the same time, these catalysts keep a high selectivity for CO methanation as compared to  $\text{CO}_2$  methanation, showing in several cases 100% selectivity in the presence of large amounts of  $\text{CO}_2$  even for very low CO concentrations (100 ppm) [10, 49–53]. Furthermore, we had demonstrated that for metal catalysts supported on reducible oxides the hydrogenation of CO and  $\text{CO}_2$  results in the formation of O-vacancies, which can strongly affect the catalytic performance of the catalysts [12,54]. These vacancies lead to pronounced electronic metal-support interactions (EMSI), which modify the electronic properties of the Ru NPs, and thus their adsorption properties for CO/ $\text{CO}_2$ . Considering the Sabatier principle, this may eventually even change the reaction mechanism or affect the competition between different reaction pathways [55]. Such effects were recently realized for the reduction of CO/ $\text{CO}_2$  on Ru/ $\text{TiO}_2$  [56–58] and Ru/ $\text{ZrO}_2$  [12,54], and also for  $\text{CO}_2$  reduction to methanol and CO on ZnO supported Au catalysts [59–61].

In the following we will, after a brief description of the experimental details, first present transient experiments, where we monitored the formation and disappearance of different surface species during the reaction upon changing from  $^{12}\text{CO}/\text{H}_2$  to  $^{13}\text{CO}/\text{H}_2$  and back by time-resolved DRIFTS (Section 3.1). This will be followed by similar type exchange measurements, changing from  $\text{CO}/\text{H}_2$  to a  $\text{CO}/\text{D}_2$  mixture (Section 3.2), and by transient measurements, monitoring the (reactive) isothermal desorption of adsorbed species upon changing from the reaction  $\text{CO}/\text{H}_2$  gas mixture to  $\text{N}_2$  or  $\text{H}_2$  at  $190^\circ\text{C}$  (Section 3.3). Next, we will use measurements of the  $\text{H}_2/\text{D}_2$  kinetic isotope effect ( $\text{KIE}_{\text{H/D}} = r_{\text{H}_2}/r_{\text{D}_2}$ ) at different temperatures to obtain further information on the nature of the rate-determining step and possible changes therein with temperature (Section 3.4). The main new findings will be summarized at the end of each section. Finally, we will briefly discuss the insights derived from these results in total in a comprehensive picture and compare them with previous mechanistic findings (Section 3.5).

## 2. Methods

### 2.1. Catalyst preparation and properties

The Ru/ $\text{TiO}_2$  catalyst was prepared by an incipient wetness impregnation method described in detail in refs. [11,51]. Briefly, a high surface area  $\text{TiO}_2$  ( $121\text{ m}^2\text{g}^{-1}$  – P90, Evonik Degussa) support was used for the preparation of 2.1 wt% Ru/ $\text{TiO}_2$  catalysts. Previous X-ray-diffraction (XRD) analysis indicated a mixed  $\text{TiO}_2$  composition, close to the rutile: anatase ratio of P90. Catalysts with Ru loadings around 2 wt% and mean particle sizes around 1.5 nm have been used in a number of

previous studies on CO methanation and were characterized carefully with respect to their physical properties already [11,12,51]. For this study, high-resolution transmission electron microscopy (HR-TEM) measurements, carried out on a Philips CM 20 electron microscope operated at 200 keV, revealed a Ru particle size distribution ranging from 1 to 2.5 nm, with a mean volume-area diameter  $d_{\text{va}}$  of 1.6 nm and a Ru dispersion of 68%.

### 2.2. Kinetic measurements - kinetic isotope effect (KIE)

The rate of CO methanation and changes therein during kinetic isotope exchange experiments and during isothermal desorption were followed in a fixed bed quartz tube micro reactor at atmospheric pressure. The pure catalyst sample was diluted with a thermally stable and catalytically inert  $\alpha\text{-Al}_2\text{O}_3$  powder (1:10 – Ru/ $\text{TiO}_2$ :  $\text{Al}_2\text{O}_3$ ) to ensure differential reaction conditions in all measurements and to avoid mass / heat transport effects. We used 200 mg of the diluted catalyst bed (1.2 cm length, diameter 0.45 cm), which resulted in maximum CO conversions of 5–7%. Prior to all experiments the diluted Ru/ $\text{TiO}_2$  catalyst was activated in the following sequence: i) heating to  $150^\circ\text{C}$  in a flow of  $\text{N}_2$  ( $40\text{ Nml min}^{-1}$ ), ii) calcination for 30 min in 10%  $\text{O}_2/\text{N}_2$  to remove adsorbed carbonate/formate-like species at this temperature, iii) purging in a flow of  $\text{N}_2$  for 15 min at  $150^\circ\text{C}$  to remove all remaining  $\text{O}_2$  after calcination, and finally iv) catalyst reduction in the reaction gas mixture (ID-ref 6000: 0.6% CO, 15.5%  $\text{N}_2$ , balance  $\text{H}_2$ ) by first heating from  $150^\circ\text{C}$  to  $190^\circ\text{C}$  and subsequent isothermal reaction at  $190^\circ\text{C}$ . According to previous X-ray photoelectron spectroscopy (XPS) and energy dispersive X-ray spectroscopy (EDX) characterization, the calcination step is sufficient to remove residual Cl from the sample after preparation (see refs. [51,52]). The partial pressures of influent and effluent gases were analyzed by on-line gas chromatography with a CO detection limit of ca. 5 ppm (DANI 86.10), using  $\text{H}_2$  as carrier gas and thermal conductivity detectors. The Ru mass-normalized  $\text{CH}_4$  formation rate was calculated from the effluent molar flow rate of  $\text{CH}_4$  formed ( $\dot{n}_{\text{CH}_4,\text{out}}$ ), according to Eq. (1), where  $m_{\text{Ru}}$  represents the mass of Ru in the catalyst.

$$r_{\text{CH}_4} = \frac{\dot{n}_{\text{CH}_4,\text{out}}}{m_{\text{Ru}}} \quad (1)$$

High purity gases were supplied by Westfalen AG (99.999%) and by Euriso-TOP ( $^{13}\text{CO}$ , 99.13%  $^{13}\text{CO}$ ).

### 2.3. In situ infrared isotope exchange measurements

Diffuse reflectance Fourier transform infrared spectroscopy (DRIFTS) measurements were carried out using a commercial in situ reaction cell (Harricks, HV-DR2, volume  $\sim 12.5\text{ cm}^3$ ), with the gas flow from the top of the cell via the catalyst bed to the bottom of the cell to achieve a rapid response at the surface of the catalyst bed. The spectra were recorded with a Nicolet 6700 spectrometer (Thermo) equipped with an MCT narrow-band detector (spectral resolution  $0.5\text{ cm}^{-1}$ ). In the initial phase, 15 scans were co-added per 1 spectrum ('quick scans', 1 spectrum every 15 s), in later stages we co-added 400 scans ('long scans', 1 spectrum every 15 min). The times given with the figures always refer to the start of the DRIFTS measurement. Switching between differently labelled reaction gas mixtures was performed by replacing the respective component via a three-ways valve. The background spectra used for normalization and background subtraction were recorded in  $\text{N}_2$  at  $150^\circ\text{C}$ , after the pretreatment procedure described in Section 2.2. As stated there, this procedure is most effective in removing adsorbed formate and carbonate species, while otherwise the spectra closely resemble those obtained after reduction in  $\text{H}_2$ . The measurements were carried out in ID-ref 6000 reformat (0.6% CO, 15.5%  $\text{N}_2$ , balance  $\text{H}_2$ ) at  $190^\circ\text{C}$  at  $41.6\text{ Nml min}^{-1}$  total flow and using 20 mg of catalyst diluted with  $\alpha\text{-Al}_2\text{O}_3$  (1:1), which was placed as a thin layer on top of a bed of pure  $\alpha\text{-Al}_2\text{O}_3$  in the DRIFTS cell. This results in a space velocity identical to that in our previous studies [10,12,51,52,58,62].

The reaction temperature given here refers directly to the temperature at the surface of the catalyst bed and was derived from the measured temperature at the sample cup via calibration measurements [63]. The IR intensities were evaluated in Kubelka-Munk units, which in most cases are approximately linearly related to the adsorbate coverage [64, 65]. Though this may result in some deviation from a linear relation with the  $\text{CO}_{\text{ad}}$  coverage of the respective CO isotopomer (see ref. [65]), it allows a direct comparison with data in our previous study [51].

The diffuse reflected FTIR intensity ( $I$ ) was converted into Kubelka-Munk units (KMUs) according to Eq. (2), where the infrared reflectance ( $R_v$ ) is calculated as the ratio of the intensity monitored during reaction ( $I$ ) to the background intensity of the catalyst ( $I_0$ ) recorded under a flow of  $\text{N}_2$  at 150 °C (Eq. (3)). Integrated intensities were determined by integrating over the respective range after background subtraction. The CO gas phase signal resulting from unreacted CO during reaction was removed from the DRIFTS spectra by subtracting a spectrum collected on an inert  $\alpha\text{-Al}_2\text{O}_3$  support under a continuous flow of 0.6%  $\text{CO}/\text{N}_2$  from the reaction spectra.

$$\text{KMU}_v = (1 - R_v)^2 / 2 R_v \quad (2)$$

$$R_v = I_v / I_{0,v} \quad (3)$$

For quantitative evaluation of the intensities we either employed a peak fitting approach (see discussion with Fig. 2) or evaluated the background corrected heights of the peaks, which for well separated bands is accurate as well (see later discussion).

### 3. Results and discussion

Before monitoring changes in the adlayer during the isotope exchange, we followed the build-up of the adlayer during reaction in a  $^{12}\text{CO}/\text{H}_2$  gas mixture at 190 °C until the system had approached a dynamic equilibrium state (150 min). As shown previously, after this time also the changes in the reaction rates are small, in particular on the time

scale of the measurements described in the following sections [51]. Spectra recorded during this initial phase (see Figure S1 in the Supporting Material (SM)) illustrate the build-up of the adlayer, with characteristic features for adsorbed  $\text{CH}_x$ , CO and formyl species, which will be discussed in detail below. They also demonstrated that the adlayer has approximately reached steady-state conditions at the end of this phase.

#### 3.1. Isotope exchange experiments: $^{12}\text{CO}/\text{H}_2 \rightarrow ^{13}\text{CO}/\text{H}_2$ and back

After equilibration in  $^{12}\text{CO}/\text{H}_2$ , we changed for 40 min from  $^{12}\text{CO}/\text{H}_2$  to a  $^{13}\text{CO}/\text{H}_2$  gas mixture to allow for a complete exchange by  $^{13}\text{C}$ -labelled species, and then returned to  $^{12}\text{CO}/\text{H}_2$ . Fig. 1a - c shows different regions of the DRIFT spectra recorded upon this change. Similar detail spectra recorded upon returning from  $^{13}\text{CO}/\text{H}_2$  to  $^{12}\text{CO}/\text{H}_2$  are presented in Fig. 1d - f.

Starting with the  $^{12}\text{CO}_{\text{ad}}$  related frequency region (1920 – 2170  $\text{cm}^{-1}$ ) (Figs. 1b and 1e), we find a number of characteristic bands under steady-state conditions, which are generally categorized into two groups. The high-frequency region includes the symmetric and asymmetric stretch vibrations of multicarbonyl species at 2138 and 2078  $\text{cm}^{-1}$ , respectively, as well as CO adsorbed on Ru sites modified by interaction with the support ('monolayer sites'), also at about 2080  $\text{cm}^{-1}$  [28,66,67]. The low-frequency region contains different on-top adsorbed  $\text{CO}_{\text{ad}}$  species (see also Table S1) in the range 1975 – 2065  $\text{cm}^{-1}$  [6,28,67,68]. Considering that upon changing to  $^{13}\text{CO}$  these bands are expected to red-shift by about 45  $\text{cm}^{-1}$  [69,70], the weak signal at 2138  $\text{cm}^{-1}$  should down-shift to about 2093  $\text{cm}^{-1}$ . This would initially be hidden in the  $^{12}\text{CO}$ -related peak at 2078  $\text{cm}^{-1}$ . Only after longer reaction in  $^{13}\text{CO}/\text{H}_2$  (after 45 min, see Fig. 1e), this signal is visible as a weak peak at about 2086  $\text{cm}^{-1}$ . Similarly, the band at 2078  $\text{cm}^{-1}$  shifts to about 2028  $\text{cm}^{-1}$ . The much higher intensity in this band as compared to the band at 2138  $\text{cm}^{-1}$  may at least partly be due to the additional presence of  $^{12}\text{CO}_{\text{ad}}$  on Ru monolayer sites. In the lower

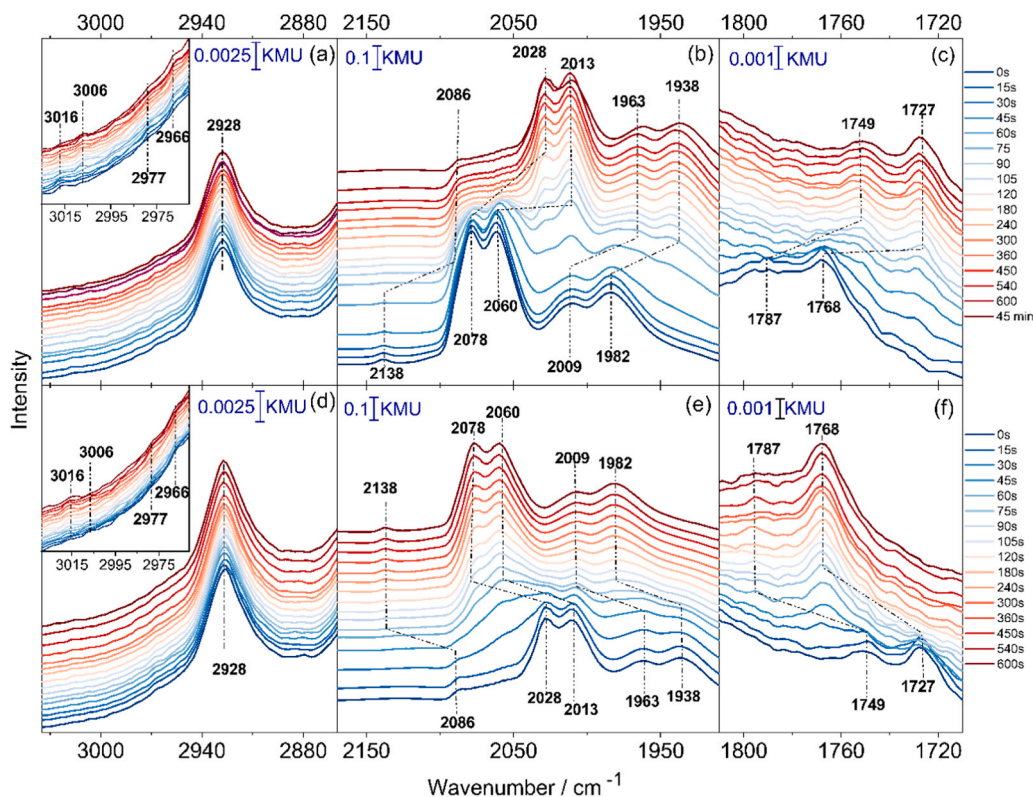


**Fig. 1.** Sequence of time-resolved ( $\Delta t = 15$  s) in situ DRIFT spectra recorded for 600 s upon switching from  $^{12}\text{CO}/\text{H}_2$  to  $^{13}\text{CO}/\text{H}_2$  gas reformate (a, b, c) at 190 °C and return (d, e, f) on a  $\text{Ru}/\text{TiO}_2$  catalyst (from bottom to top: 0, 15, 30, 45, 60, 75, 90, 105, 120, 180, 240, 300, 360, 450, 540, 600 s, and, for (a), (b), and (c), 45 min).

frequency range, the band appearing at  $2060\text{ cm}^{-1}$  shifts to  $2011\text{ cm}^{-1}$ . The second band at  $2009\text{ cm}^{-1}$  shifts to  $1963\text{ cm}^{-1}$ , and the band at  $1982\text{ cm}^{-1}$  shifts to  $1938\text{ cm}^{-1}$ , in good agreement with expectations for the isotope induced red-shift (see above). All absorption bands of the  $^{13}\text{CO}$  species return to their original position and intensity upon switching back from  $^{13}\text{CO}/\text{H}_2$  to  $^{12}\text{CO}/\text{H}_2$ .

In the region characteristic for adsorbed formyl ( $\text{HCO}_{\text{ad}}$ ) species we find a weak band at  $1768\text{ cm}^{-1}$  (Figs. 1c and 1f), which is attributed to adsorbed formyl species resulting from the hydrogenation of adsorbed CO [71–73]. This band shifts to  $1727\text{ cm}^{-1}$  in  $^{13}\text{CO}/\text{H}_2$ . Moreover, there is also a very weak signal at  $1787\text{ cm}^{-1}$  in  $^{12}\text{CO}/\text{H}_2$ , which shifts to  $1749\text{ cm}^{-1}$  in  $^{13}\text{CO}/\text{H}_2$ . This latter band was not resolved in previous studies of CO methanation on other Ru catalysts such as Ru/ $\text{Al}_2\text{O}_3$  [12, 18], Ru/ $\text{ZrO}_2$  [12], or Ru/zeolite [53]. It was, however, detected with measurable intensity during the initial 350 min of the reaction on Ru/ $\text{TiO}_2$  [11], which fits to the present observations at much shorter reaction times. In contrast, the main band at  $1768\text{ cm}^{-1}$  was found to be stable over 1000 min time on stream [11]. Most likely, the band at  $1787\text{ cm}^{-1}$  is due to adsorbed formyl species on different adsorption sites, which leads to a small difference in the frequency [72,73]. Considering the similar magnitude of the IR excitation cross section of CO and HCO radicals in matrix isolation experiments [74,75], the coverage of  $\text{HCO}_{\text{ad}}$  must be much less than that of  $\text{CO}_{\text{ad}}$ .

In Fig. 1a, d we show the region of the C-H stretch vibrations, which is dominated by a band at  $2928\text{ cm}^{-1}$ . Bands at this frequency have previously been assigned to the symmetric C-H stretch vibration of  $\text{CH}_2$  groups in alkanes [76] and also to the C-H bending vibration of formyl species on Ru(0001) [71]. This signal grows steadily in intensity during the initial  $\sim 100$  min (Figure S1a), and then remains at this level. Furthermore, it does not shift upon the isotope exchange, different from the bands related to  $\text{CO}_{\text{ad}}$  and  $\text{HCO}_{\text{ad}}$  (Figure S1a). In combination, these observations indicate that the related species is not a reaction intermediate in the dominant pathway, such as  $\text{HCO}_{\text{ad}}$ , but rather a side product of the reaction or a spectator species whose population saturates. We tentatively relate this band to  $\text{CH}_2$  groups in adsorbed alkyls [76] or in ether ( $\text{O}-\text{CH}_2-$ ) or dioxyethylene ( $\text{H}_2\text{CO}_2$ ) species on the  $\text{TiO}_2$  substrate [77]. In addition to this dominant band, there are very weak signals at  $3016$  and  $2977\text{ cm}^{-1}$ , which shift to  $3006$  and  $2966\text{ cm}^{-1}$  in  $^{13}\text{CO}/\text{H}_2$ , respectively, and which were assigned previously to C-H vibrations in (mostly) gas phase  $\text{CH}_4$  and in  $\text{CH}_{3,\text{ad}}$  species, respectively (see inset in Fig. 1a, d) [18,49,78]. These bands seem to represent reactive intermediates in the reaction pathway. Monitoring the exchange in gas phase  $\text{CH}_4$  product species by mass spectrometry was not possible from experimental reasons. Finally, there were no significant changes in the O-H region between  $3200$  and  $3600\text{ cm}^{-1}$ .

To get more insight into the role of the different adsorbed species in the reaction, we quantitatively evaluated the decay of the different vibrational bands and their re-appearance upon returning to  $^{12}\text{CO}/\text{H}_2$ , which reflects the loss (increase) of  $^{12}\text{CO}$ -related species during reaction upon transition to a  $^{13}\text{CO}/\text{H}_2$  ( $^{12}\text{CO}/\text{H}_2$ ) gas phase, due to desorption and/or reaction of the respective species, while the total coverage of the respective  $\text{CO}_{\text{ad}}$  related species remains approximately constant. Because of the overlap between different vibrational bands related to  $^{12}\text{CO}_{\text{ad}}$  and  $^{13}\text{CO}_{\text{ad}}$ , an unambiguous straightforward evaluation was only possible for the band at  $2138\text{ cm}^{-1}$ . The temporal evolution of the intensity of that signal is presented in Fig. 2a. Here, complete exchange at this state is reached within about 60–90 s after starting the exchange of the gas phase. (Note that this conclusion will not be affected by small deviations of the KMU intensity from a linear relationship with  $\text{CO}_{\text{ad}}$  coverage.) Second, the exchange of this  $\text{CO}_{\text{ad}}$  signal is essentially on the same time scale as that of the CO gas phase DRIFTS signal, which takes slightly less than 60 s (see inset in Fig. 2a).

Comparing the  $\text{CO}_{\text{ad}}$  related spectra in Fig. 1b shows that they can largely be reproduced by a linear combination of the first spectrum (pure  $^{12}\text{CO}_{\text{ad}}$ ) and the last spectrum (complete exchange to  $^{13}\text{CO}_{\text{ad}}$ ). Examples for such kind of linear combination analysis (LCA) are illustrated for

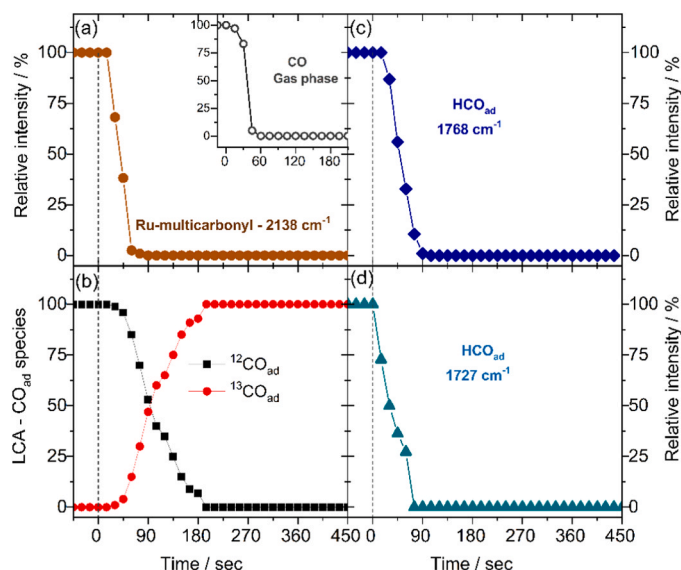


**Fig. 2.** Relative intensities of the bands related to adsorbed  $^{12}\text{CO}$  and adsorbed  $\text{H}^{12}\text{CO}$  (formyl) species (see figure) as a function of time upon the isotope exchange from  $^{12}\text{CO} / \text{H}_2$  to  $^{13}\text{CO} / \text{H}_2$ . The relative intensity is the integrated intensity of the respective band normalized by the initial intensity at  $t = 0$  s (intensity of the first spectrum from the bottom in Fig. 1). Data points at  $t < 0$  s represent the steady-state intensity (spectra are not included in Fig. 1). The inset in panel (a) shows the decay of  $^{12}\text{CO}$  gas phase intensity based on the decay of the integrated intensity of the R-branch (from  $2145$  to  $2235\text{ cm}^{-1}$ ). The relative intensities in b) are derived from the LCA analysis (see text).

three different spectra in Fig. 3. Closer inspection reveals, however, that there are also slight differences. For instance, the multicarbonyl band has completely disappeared in the measured spectrum already after 75 s, while there is still a clear peak visible in the simulated one. Furthermore, there are subtle differences in the intensity ratio between the peaks at  $2028$  and  $2011\text{ cm}^{-1}$ . In general, however, the resulting agreement is very good. Hence, there is almost no change in the relative population of the different on-top adsorbed  $\text{CO}_{\text{ad}}$  species, except for the multicarbonyl species. The resulting decay of the total  $^{12}\text{CO}_{\text{ad}}$  related

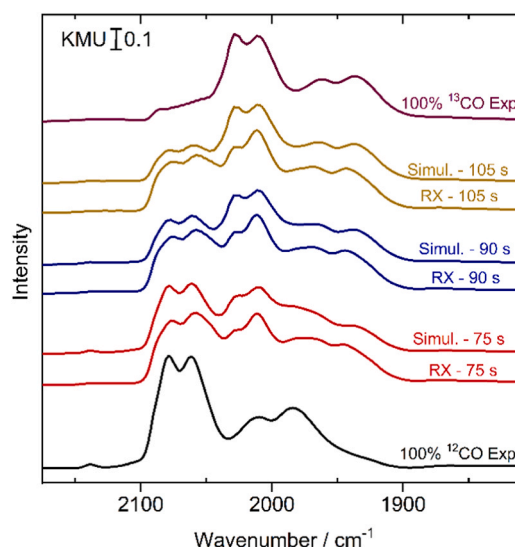


**Fig. 3.** Examples for the linear combination analysis (LCA) of the spectra recorded after 75 s, 90 and 105 s (see Fig. 1) after gas exchange to  $^{13}\text{CO}/\text{H}_2$ , showing the measured and simulated spectra. Spectra recorded before exchange ( $^{12}\text{CO}_{\text{ad}}$ , black) and after complete exchange ( $^{13}\text{CO}$ , green) were used as references.

signal and the simultaneous increase of the  $^{13}\text{CO}_{\text{ad}}$  related signal, as derived from the compositions of the simulated spectra, are displayed in Fig. 2b. As already mentioned above, the decay of the total  $^{12}\text{CO}_{\text{ad}}$  signal is somewhat slower than that of the  $^{12}\text{CO}$  multicarbonyl signal at  $2138\text{ cm}^{-1}$ , which points to a lower reaction rate / desorption rate of these species as compared to the multicarbonyls. The differences are, however, small when comparing with the decay time observed during desorption (see over next section), which we will discuss later. Because of the high surface mobility of adsorbed CO species and the rapid exchange between different  $\text{CO}_{\text{ad}}$  species, the slower exchange cannot easily be converted into desorption/reaction rates of different types of adsorbed CO.

For the formyl species with its dominant band at  $1768\text{ cm}^{-1}$  and a weaker band at  $1727\text{ cm}^{-1}$ , complete exchange also occurs within about 60 s, i.e., on the same time scale as the gas phase exchange and the multicarbonyl exchange (Figs. 2b and 2c). This conclusion is not affected by the fact that due to the rather complex deconvolution of the bands the intensities were evaluated from the peak heights. Hence, both multicarbonyl exchange and  $\text{HCO}_{\text{ad}}$  exchange follow closely the change in CO isotope composition of the gas phase, while exchange of the other  $\text{CO}_{\text{ad}}$  species is somewhat slower. Reasons for that will be discussed more later. Qualitatively, this would fit to a picture where the formation of  $\text{HCO}_{\text{ad}}$  intermediates mainly results from multicarbonyl hydrogenation. Here we would like to note that because of the much smaller signal intensity and the resulting larger possible errors in the evaluation the actual time for complete exchange of  $\text{H}^{12}\text{CO}_{\text{ad}}$  may be somewhat larger. From the rapid exchange measured for these species we conclude that removal of  $\text{CO}_{\text{ad}}$  and  $\text{HCO}_{\text{ad}}$  is fast, close to that of the gas phase, and that  $\text{CO}_{\text{ad}}$  and  $\text{HCO}_{\text{ad}}$  are essentially in (dynamic) equilibrium with each other and with the gas phase. In that case the relative populations of  $\text{CO}_{\text{ad}}$  and  $\text{HCO}_{\text{ad}}$  are largely determined by their relative thermodynamic stability. According to the definition given by Boudart [79], this would mean that the rate-determining step follows after these reaction steps, i.

e., after CO adsorption and its hydrogenation to  $\text{HCO}_{\text{ad}}$ .

Finally, one can compare these exchange times with that of the final product  $\text{CH}_4$ . Since GC measurements cannot distinguish between  $^{12}\text{CH}_4$  and  $^{13}\text{CH}_4$  and since the DRIFTS signals of gas phase  $\text{CH}_4$  are very weak, a quantitative evaluation is not possible. On a qualitative scale, however, the disappearance of the  $\text{CH}_4$  related band at  $3016\text{ cm}^{-1}$  seems to be on a similar time scale as the disappearance of the  $\text{CO}_{\text{ad}}$  and  $\text{HCO}_{\text{ad}}$  signals.

Main findings of these experiments are that during reaction a number of adsorbed species exist on the surface, including CO multicarbonyls, different  $\text{CO}_{\text{ad}}$  species and  $\text{HCO}_{\text{ad}}$  species, and that all of them undergo  $^{12}\text{C}$  to  $^{13}\text{C}$  exchange. From the rapid exchange of the respective isotopologues removal of  $\text{CO}_{\text{ad}}$  and  $\text{HCO}_{\text{ad}}$  seems to be fast and  $\text{CO}_{\text{ad}}$  and  $\text{HCO}_{\text{ad}}$  are in equilibrium with each other and with the gas phase. The band at  $2928\text{ cm}^{-1}$ , which is not affected by the CO exchange, reflects side products / spectator species that were formed until reaching steady state conditions in  $^{12}\text{CO}/\text{H}_2$ . We cannot decide from these data, however, whether the  $\text{CO}_{\text{ad}}$  removal occurs mainly via  $\text{CO}_{\text{ad}}$  desorption or via  $\text{CO}_{\text{ad}}$  hydrogenation, or on differences in the reactivity of the different adsorbed CO species. Due to the high surface mobility of  $\text{CO}_{\text{ad}}$  species these are expected to be in a 2D equilibrium, where removal of a specific  $\text{CO}_{\text{ad}}$  species results in rapid re-equilibration of the remaining ones.

### 3.2. Isotope exchange experiments: $^{12}\text{CO}/\text{H}_2 \rightarrow ^{12}\text{CO}/\text{D}_2$ and back

In a similar experiment, we followed changes in the adlayer upon changing from  $^{12}\text{CO}/\text{H}_2$  to  $^{12}\text{CO}/\text{D}_2$  and vice versa. The resulting sequences of spectra are presented in Fig. 4a - c (exchange from  $^{12}\text{CO}/\text{H}_2$  to  $^{12}\text{CO}/\text{D}_2$ ) and Fig. 4d - f (re-exchange from  $^{12}\text{CO}/\text{D}_2$  to  $^{12}\text{CO}/\text{H}_2$ ). This aims mainly at the identification of different C-H containing adsorbates formed during reaction. We are particularly interested in an unambiguous clarification of whether in addition to formyl species also adsorbed

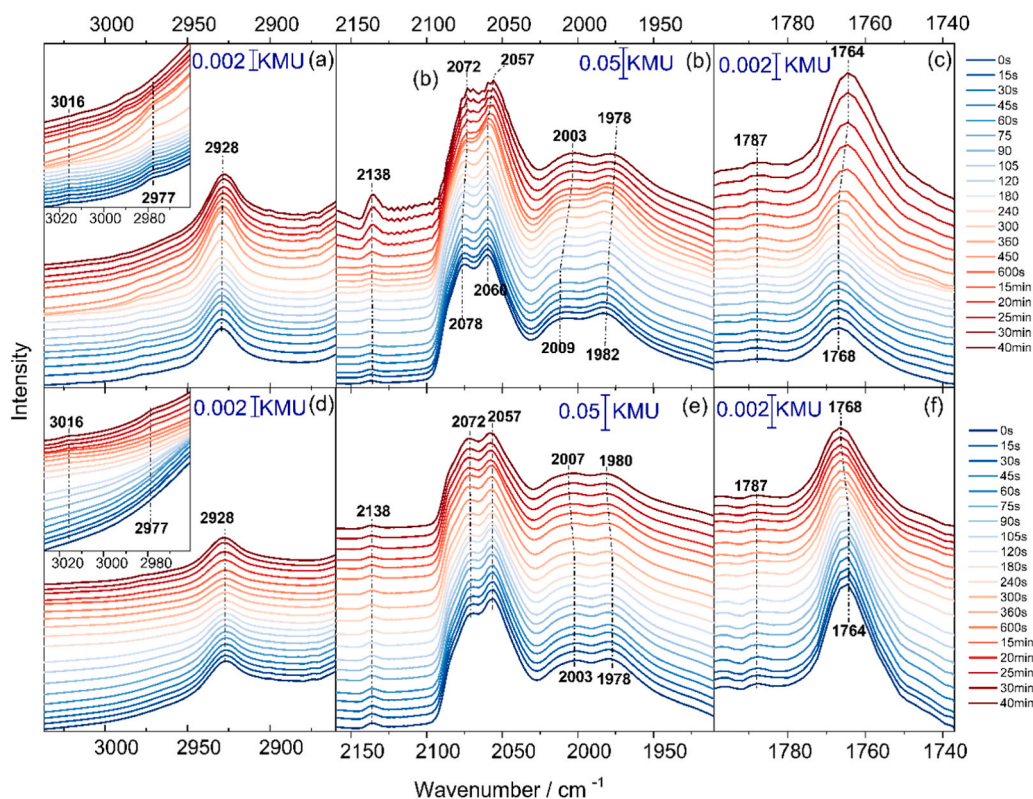


Fig. 4. Sequences of time-resolved ( $\Delta t = 15\text{ s}$ ) in-situ spectra recorded during CO methanation at  $190\text{ }^{\circ}\text{C}$  on the  $\text{Ru}/\text{TiO}_2$  catalyst upon switching from  $^{12}\text{CO}/\text{H}_2$  to  $^{12}\text{CO}/\text{D}_2$  reformat gas (a, b) and vice versa (c, d) (times as indicated in the figure).

formate species are formed or whether these can be excluded as reaction intermediates. This can be decided by the unique D-C stretch vibration of adsorbed DCOO at  $2190\text{ cm}^{-1}$  [80].

In a first view, there seems to be little change in the general appearance of the spectra upon switching. Closer inspection reveals, however, two significant differences. First, the  $\text{CO}_{\text{ad}}$  related bands show a red shift of  $\sim 5-7\text{ cm}^{-1}$  upon changing from  $\text{H}_2$  to  $\text{D}_2$  (Fig. 4b, c) and reverse when going back from  $\text{D}_2$  to  $\text{H}_2$ , which would not have been expected. This shift can result, e.g., from co-adsorbate induced changes in the CO adsorption properties, e.g., in a CO-H adsorption complex, and the resulting changes in the zero-point energy. Interestingly, there was no measurable shift for the multicarbonyl peak at  $2138\text{ cm}^{-1}$ , which may be due to the saturation of this site by two  $\text{CO}_{\text{ad}}$  species, which inhibits co-adsorption with  $\text{H}_{\text{ad}}$  or  $\text{D}_{\text{ad}}$  and therefore  $\text{D}_{\text{ad}}$  induced frequency shifts. On the other hand, this band increases significantly in intensity upon changing to  $\text{D}_2$ . Since there is no reason for expecting significant changes in the cross section for IR excitation, this must reflect considerable change in coverage of these species. As a speculation, the lower coverage in  $\text{CO}/\text{H}_2$  may be caused by more pronounced competitive adsorption of  $\text{H}_{\text{ad}}$  on these sites than obtained for the weakly bound  $\text{D}_{\text{ad}}$  in  $\text{CO}/\text{D}_2$ . Second, the  $\text{HCO}_{\text{ad}}$  band at  $1768\text{ cm}^{-1}$  shifts by  $\sim 4\text{ cm}^{-1}$ . Despite the similar sizes of the red-shifts for  $\text{CO}_{\text{ad}}$  and  $\text{HCO}_{\text{ad}}$ , the physical reason for this must be different from that observed for  $\text{CO}_{\text{ad}}$ . In this case, it must result from an intramolecular effect, namely the bonding of the H(D) atom to the C atom of  $\text{HCO}_{\text{ad}}$ , which affects also the vibrational frequency of the C=O group. Considering the small effect of replacing H by D in  $\text{HCO}_{\text{ad}}$  on the C-O bond, we do not expect significant shifts, though a more detailed discussion of this shift is not possible because of the lack of theoretical studies. Also, because of the small shifts, a quantitative evaluation of the disappearance/appearance of the respective bands similar to that upon  $\text{H}_2/^{12}\text{CO} - \text{H}_2/^{13}\text{CO}$  is not possible in this case. Furthermore, the intensity of the C=O band increased by almost a factor of  $\sim 2$  when changing from  $\text{HCO}_{\text{ad}}$  to  $\text{DCO}_{\text{ad}}$ , and this increase disappears reversibly when going back to  $\text{CO}/\text{H}_2$  (Fig. 5). From similar reasons as stated above, we also do not expect significant differences in the cross-sections for IR excitations of these two species. Therefore, the significant increase in intensity must be due to a significantly higher coverage of  $\text{DCO}_{\text{ad}}$  than obtained for  $\text{HCO}_{\text{ad}}$ . Such significant increase in steady-state coverage can simply be explained by kinetic isotope effects in the rates for hydrogen adsorption and  $\text{HCO}_{\text{ad}}$  decomposition and  $\text{HCO}_{\text{ad}}$  hydrogenation as compared to  $\text{DCO}_{\text{ad}}$ , as they were described by Ojeda et al. for the Fischer-Tropsch synthesis on Fe(110) model surfaces [26].

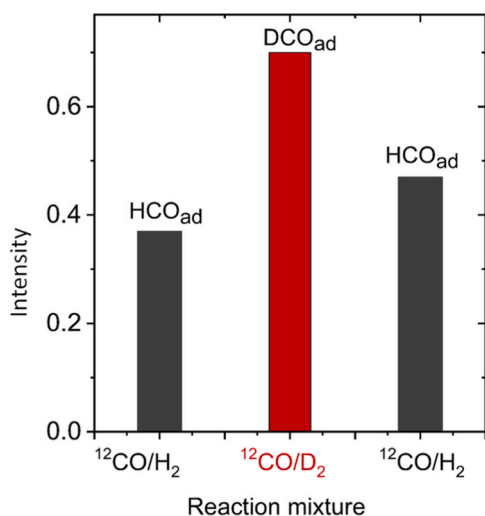


Fig. 5. Integrated intensity (in  $10^{-2}\text{ KMU}\cdot\text{cm}^{-1}$ ) of the  $\text{HCO}_{\text{ad}}$  related band at  $1768\text{ cm}^{-1}$  under steady-state conditions in  $^{12}\text{CO}/\text{H}_2$  and  $^{12}\text{CO}/\text{D}_2$  before and after switching from  $^{12}\text{CO}/\text{H}_2$  to  $^{12}\text{CO}/\text{D}_2$  and back again at  $190^\circ\text{C}$ .

Finally, we checked for variations in the spectral region between  $1250$  and  $1600\text{ cm}^{-1}$ , since bands in this range would be characteristic for adsorbed formate species, but did not find any significant changes (see Figure S2). We also tested the range characteristic for C-H stretch vibrations. As illustrated in Figs. 4a and 4d, there are weak signals of adsorbed gas phase  $\text{CH}_4$  and  $\text{CH}_{\text{x,ad}}$  species at  $3016$  and  $2977\text{ cm}^{-1}$ , respectively (see discussion in 3.1), but no indications of adsorbed formate species or deuterated formate species, which would appear at ca.  $2870\text{ cm}^{-1}$  or  $2190\text{ cm}^{-1}$  [80], respectively. Since we found the latter signals to be very sensitive in test measurements, we can essentially rule out the formation of adsorbed formate species under present reaction conditions, and in particular their participation in the reaction as reaction intermediate.

Main findings of this section are that we can essentially rule out the formation of adsorbed formate species and their participation in the reaction as reaction intermediate under present reaction conditions, and the significant increase in the  $\text{DCO}_{\text{ad}}$  band intensity compared to the  $\text{HCO}_{\text{ad}}$  band upon changing to  $\text{CO}/\text{D}_2$ .

### 3.3. Desorption and methanation of adsorbed intermediates in $\text{N}_2$ and $\text{H}_2$

For more information on the question whether the decay of the  $^{12}\text{C}$ -related species arises mainly from reaction with hydrogen or from desorption of the respective species, we performed similar measurements as before, but switching now from  $^{12}\text{CO}/\text{H}_2$  to a continuous flow of  $\text{N}_2$  or  $\text{H}_2$ , respectively. When comparing with the isotope exchange experiments presented before, it is important to note that in the present case the total coverages of the different species will decrease with time, whereas in the isotope exchange experiments only the (non-)labelled part decreased, while the total coverage essentially remained constant. Also for these experiments we obtained reproducible trends in different experiments.

#### 3.3.1. Desorption and methanation of adsorbed intermediates in $\text{N}_2$

DRIFT spectra recorded during desorption, upon switching from the reaction gas mixture to a flow of  $\text{N}_2$ , are shown in Fig. 6; the temporal evolution of the integrated intensities of the  $\text{CO}_{\text{ad}}$  related bands (all bands) and of the  $\text{HCO}_{\text{ad}}$  band, respectively, are plotted in Fig. 7b. Obviously, the decay behavior of the  $^{12}\text{CO}_{\text{ad}}$  related bands is very different from that observed during the isotope exchange experiment. Even after 30 min, there is almost no change in the total intensity. In contrast, the small band at  $2138\text{ cm}^{-1}$  related to the multicarbonyl species had disappeared after a couple of minutes. Hence, this species, which based on the peak intensity is present only in small amounts, is less stable than the on-top adsorbed  $\text{CO}_{\text{ad}}$  and desorbs more rapidly. This fits also to our previous observation of a faster exchange of this species (Fig. 1). Over longer times, also the main signal loses in intensity, with some differences in the different bands. Complete desorption of  $\text{CO}_{\text{ad}}$  is reached only after about 4 h (Fig. 6e). For comparison, in the isotope exchange experiment the decay of the  $^{12}\text{CO}_{\text{ad}}$  species from the steady-state coverage and the simultaneous build-up of the  $^{13}\text{CO}_{\text{ad}}$  species were completed within about 180 s (Figs. 1 and 2).

On the other hand, the  $\text{HCO}_{\text{ad}}$  intermediate disappeared almost completely in about 4 min during desorption in  $\text{N}_2$  (Fig. 6c). This is somewhat slower than in the isotope exchange experiment (about 90 s), but on the same order of magnitude. Evidently, desorption / decomposition of the  $\text{HCO}_{\text{ad}}$  intermediate in  $\text{N}_2$  is significantly faster than that of  $\text{CO}_{\text{ad}}$  species, which is different from the about similar decay times of these species during isotope exchange. Note that this conclusion is not affected by the time required for gas exchange in the reaction cell of about 60 s. Looking at the  $\text{CH}_{\text{x}}$  species, the intensity for the C-H stretch in  $\text{CH}_4$  species ( $3016\text{ cm}^{-1}$ ) decayed very quickly, within less than 60 s, as would be expected for weakly bound product species in the absence of further formation of this species. In contrast, the band of spectator  $\text{CH}_2$ -containing alkyl or other species at  $2929\text{ cm}^{-1}$  decreased at a much slower rate and disappeared completely only after than 120 min

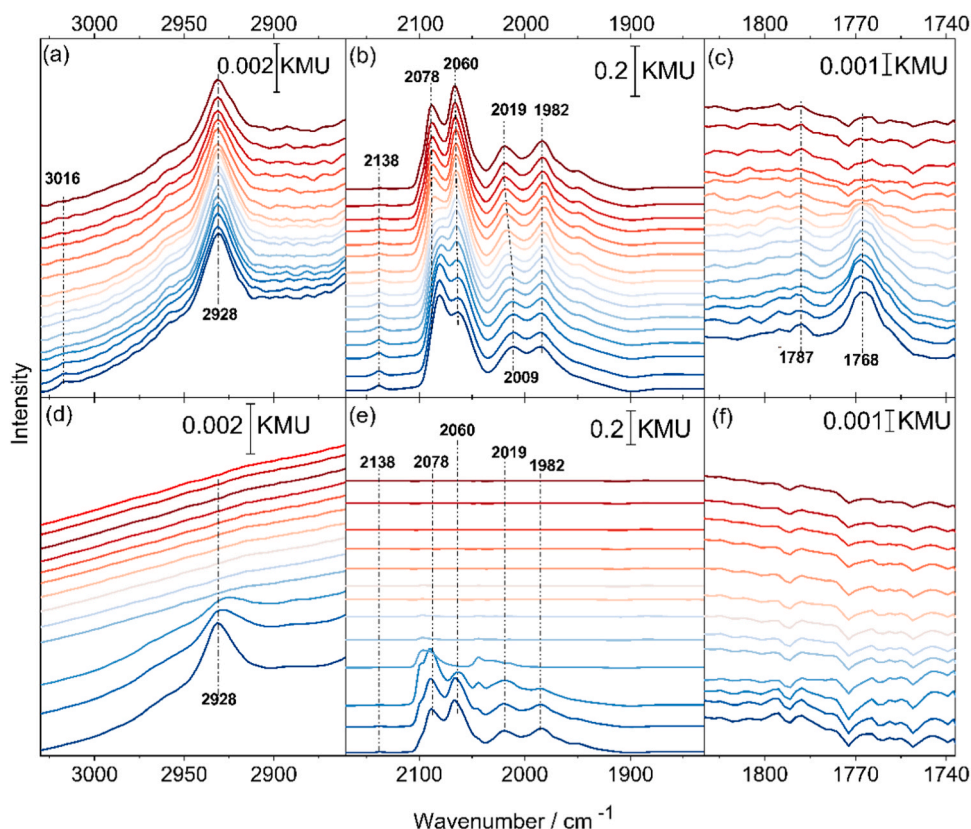


**Fig. 6.** : Series of in situ DRIFTS spectra recorded over 1000 min during isothermal desorption at 190 °C in N<sub>2</sub>, after changing from ID-ref 6000 reformat gas to a flow of pure N<sub>2</sub> at 190 °C. Spectra recorded during the first 10 min are presented in the upper panels (a, b, c, from bottom to top: 0, 15, 30, 45, 60, 75, 90, 105, 120, 180, 240, 300, 360, 450, 540 and 600 s). Spectra recorded at extended desorption times are presented in the lower panels (d, e, f, from bottom to top: 15, 30, 60, 120, 230, 290, 350, 410, 530, 650, 770, 890, 1010 min).

(Fig. 6d). The long lifetime of this latter species at 190 °C points to a rather strong adsorption bond of this species.

The generally much slower decay of the different CO<sub>ad</sub> species during isothermal desorption in N<sub>2</sub> compared to the corresponding isotope exchange experiment (Fig. 1) can be explained in two ways. Either it is mainly caused either by faster reactive CO<sub>ad</sub> consumption in the isotope exchange experiment, by reaction with hydrogen, or by faster desorption. While faster hydrogenation in the isotope exchange experiment is straightforward, faster desorption therein could also be possible. It can result from a CO<sub>ad</sub> coverage effect, caused by a rapid decrease of the CO desorption rate with decreasing CO<sub>ad</sub> coverage during desorption. Assuming first order desorption / reaction kinetics, and considering that the barrier is in the exponential, this effect can be much more pronounced than effects caused by the lower CO<sub>ad</sub> coverage itself. Such kind of strongly decreasing CO<sub>ad</sub> adsorption energy with higher coverages, due to decreasing CO<sub>ad</sub> – CO<sub>ad</sub> repulsive interactions, is well known for CO adsorption on Ru(0001) [81]. It will lead to an increasingly lower desorption rate with lower CO<sub>ad</sub> coverage in the isothermal desorption experiment. Since different from the isotope exchange experiment there are only <sup>12</sup>CO species involved in this experiment, exchange between different sites does not play a role here. Hence, at this point we cannot discriminate between the two possibilities, slower CO<sub>ad</sub> reaction or slower CO<sub>ad</sub> desorption in the desorption experiment, but will return to this in the next section.

The rapid decay of the formyl band in the N<sub>2</sub> atmosphere, in contrast, must be due to rapid HCO<sub>ad</sub> desorption or re-conversion into CO<sub>ad</sub>. Further reaction with co-adsorbed H<sub>ad</sub> and subsequent desorption of the resulting products (formaldehyde, methane) is hardly possible, since because of the high temperature H<sub>ad</sub> will desorb quickly upon switching to N<sub>2</sub>, at least on a time scale of 3–4 min. This will be discussed in more detail in below in this section.

Finally, we compared the time evolution of the coverage of these adsorbed reaction intermediates with that of the CH<sub>4</sub> formation rate during desorption in N<sub>2</sub>. For these measurements the GC was connected to the outlet of the DRIFTS cell. Fig. 7a shows the Ru mass normalized CH<sub>4</sub> formation rates during desorption in N<sub>2</sub> (filled symbols), while in Fig. 7b we plotted the time evolution of the relative intensities of the CO<sub>ad</sub> species (total intensity) and of the HCO<sub>ad</sub> intermediate over 150 min on stream. Within 2 min after changing from CO/H<sub>2</sub>/N<sub>2</sub> to pure N<sub>2</sub>, the CH<sub>4</sub> concentration and thus the rate of CH<sub>4</sub> production had dropped to zero. (Note that the time of 2 min is an upper limit, as there are no GC measurements directly before and after the switch.) This fully agrees with the rapid decay of the CH<sub>4,ad</sub> related band. The decay of the CH<sub>4</sub> formation rate is even faster than that of the adsorbed formyl related band (decay in about 3–4 min, see Fig. 7b). Considering that the complete gas exchange takes 1 min at most (see Fig. 2a), this means that we have no evidence for CH<sub>4</sub> formation by ongoing reaction of H<sub>ad</sub> with adsorbed reaction intermediates that were formed before switching to N<sub>2</sub>. This is consistent also with the very short lifetime of H<sub>ad</sub> at 190 °C.

The main findings of this section are the much slower decay of the CO<sub>ad</sub> coverage in N<sub>2</sub> as compared to the isotope exchange experiment, with about 50% of the initial intensity being left even after 1 h. In contrast, the intensity decay of the CO multicarbonyls and of the adsorbed formyl species is only slightly slower than their decay under reaction conditions. We explained this by either predominant reactive CO<sub>ad</sub> removal during the isotope exchange experiments, by CO<sub>ad</sub> hydrogenation, or by a rapid decrease of the CO<sub>ad</sub> desorption rate with decreasing CO<sub>ad</sub> coverage due to stabilization of the CO<sub>ad</sub>, which slows down CO desorption in the CO<sub>ad</sub> desorption measurement. Considering also the fast reaction of CO<sub>ad</sub> to HCO<sub>ad</sub> in the isotope exchange experiment (rapid exchange in Fig. 1c), both effects are likely to contribute to the slower removal of CO<sub>ad</sub> during the desorption experiment. In

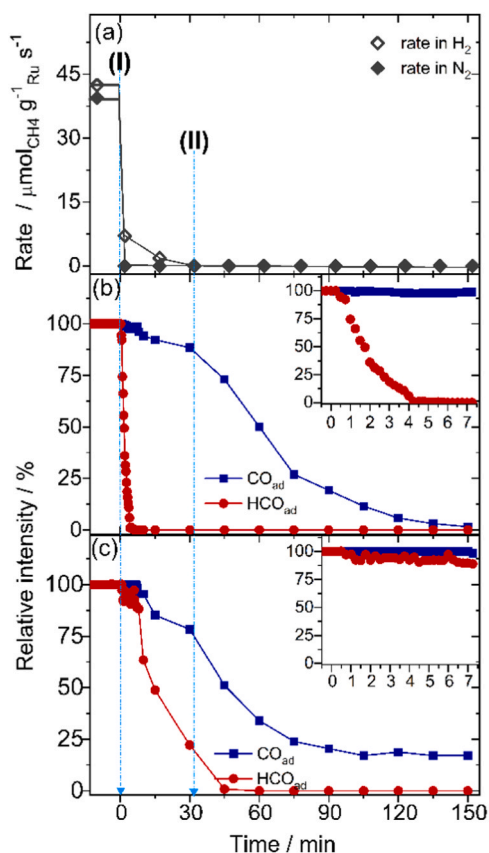


**Fig. 7.** (a) CH<sub>4</sub> formation rate (GC) upon isothermal desorption in N<sub>2</sub> or H<sub>2</sub>, changing from ID-ref 6000 (0.6% CO, 15.5% N<sub>2</sub>, H<sub>2</sub>) reformat to N<sub>2</sub> (filled black symbols) or to H<sub>2</sub> (open symbols) at 190 °C. (b, c) Relative total intensity of the CO<sub>ad</sub> related bands (blue squares) and of the HCO<sub>ad</sub> related bands (1768 and 1784 cm<sup>-1</sup>, red circles) during desorption in N<sub>2</sub> (b) and in H<sub>2</sub> (c), respectively, after surface saturation in ID-ref 6000 gas mixture at 190 °C. Insets in panels b) and c) show the decay with higher time resolution (time scale 0 - 450 s). Dashed blue lines indicate the times when the reactant stream was switched (I) and CH<sub>4</sub> formation in H<sub>2</sub> was no more detected (II). Because of the manual synchronization between gas stream switching and GC / IR measurements, the precision of the time scales of the GC and DRIFTS measurements is about 15 s.

contrast, the much faster coverage decay of adsorbed formyl species under desorption conditions (in N<sub>2</sub>) than in a flow of H<sub>2</sub> must mainly be caused by the inhibition of further HCO<sub>ad</sub> formation from CO<sub>ad</sub> and H<sub>ad</sub> in the absence of H<sub>2</sub>/H<sub>ad</sub> in a N<sub>2</sub> atmosphere, rather than from a faster desorption / decomposition in that atmosphere. Finally, the very slow decay of the C-H vibration in CH<sub>2</sub>-containing species such as alkyl or ether groups (2928 cm<sup>-1</sup>), which takes about 1 h to disappear completely in N<sub>2</sub>, supports our earlier conclusion that this species acts as a rather strongly bound spectator and is not involved in the main reaction pathway.

### 3.3.2. Desorption and methanation of adsorbed intermediates in H<sub>2</sub>

To test the impact of hydrogen on the desorption and hydrogenation behavior of the adsorbed reaction intermediates, we also followed the decay of the band intensities of these species during exposure to a stream of H<sub>2</sub> (100% H<sub>2</sub>, 190 °C), by switching to a H<sub>2</sub> atmosphere after the adlayer had been saturated for 150 min in an ID-ref 6000 reaction mixture. Representative DRIFT spectra are shown in Fig. 8, the intensity decay of the CO<sub>ad</sub> and adsorbed formyl related bands during desorption / further reaction is plotted in Fig. 7c.

Similar to desorption in the N<sub>2</sub> atmosphere, removal of CO<sub>ad</sub> is rather slow. After 1 h about 70% have desorbed, and most of the adsorbed CO

has disappeared only after about 4 h. Nevertheless, in the initial phase the loss of CO<sub>ad</sub> intensity is somewhat faster than during desorption in N<sub>2</sub>. On the other hand, different from desorption in N<sub>2</sub>, small amounts are still present after 1010 min, as indicated by weak bands at 2017 and 2075 cm<sup>-1</sup>. The remaining intensity in this band (about 20 – 25% of the initial intensity), which is not observed during desorption in N<sub>2</sub>, may, e. g., be due to an H<sub>ad</sub>-induced stabilization of these CO<sub>ad</sub> species, which can only occur at low CO<sub>ad</sub> coverages and not during the SSTKA-DRIFTS experiment. Hence, CO<sub>ad</sub> removal is not only slow under isothermal desorption conditions in N<sub>2</sub> (see last section), but at low CO<sub>ad</sub> coverage also for reactive removal by CO<sub>ad</sub> hydrogenation. This supports our previous proposal that CO<sub>ad</sub> removal is slowed down by a CO<sub>ad</sub> coverage effect, which affects not only the CO<sub>ad</sub> desorption rate, but also the CO<sub>ad</sub> hydrogenation rate. Hence, both the barrier for desorption and the reaction barrier are raised upon the stabilization of the CO<sub>ad</sub> at lower CO<sub>ad</sub> coverage (initial state stabilization). In contrast, in the isotope exchange experiment, where the CO<sub>ad</sub> coverage is constant and high, this does not happen, and CO<sub>ad</sub> removal can be fast. The physical origin of this H<sub>ad</sub> induced stabilization is so far unclear and can only be speculated upon. Finally, we note that also in this case removal of the multicarbonyl related band at 2138 cm<sup>-1</sup> is fast, taking place in the first few minutes. As discussed before, this reflects the lower stability of this species compared to the other CO<sub>ad</sub> species.

Moving on to the hydrogenation products, the bands of the C-H stretch vibration in gas phase CH<sub>4</sub> (3016 cm<sup>-1</sup>) and in CH<sub>3,ad</sub> (2977 cm<sup>-1</sup>) are too low in intensity to be resolved. The rather strong band of the C-H vibration in CH<sub>2</sub>-containing species at 2928 cm<sup>-1</sup> takes again about 1 h to disappear completely, which is comparable to the desorption behavior in N<sub>2</sub>.

The band related to the C=O vibration of HCO<sub>ad</sub> seems to be much more stable during desorption in H<sub>2</sub> than in N<sub>2</sub>. It took about 30 – 45 min to completely disappear, compared to 3 – 4 min during desorption in N<sub>2</sub>. Reasons for the much slower HCO<sub>ad</sub> removal will be discussed in the next paragraph.

Finally, we again compare the decay of the adlayer related signal intensities with the time evolution of the CH<sub>4</sub> formation rate. Fig. 7a shows that after switching to H<sub>2</sub> the Ru mass normalized CH<sub>4</sub> formation rate decreased by about a factor of 6, from 40 to 7.1  $\mu\text{mol}_{\text{CH}_4} \text{g}^{-1} \text{Ru} \text{s}^{-1}$ , in the first 2 min after the gas exchange, while the CO<sub>ad</sub> coverage remained almost constant. The intensity of the HCO<sub>ad</sub> intermediate had decayed somewhat. At the next GC measurement, 17 min after switching, the CH<sub>4</sub> formation rate had decayed further to 1.5  $\mu\text{mol}_{\text{CH}_4} \text{g}^{-1} \text{Ru} \text{s}^{-1}$  (CO<sub>ad</sub> intensity: about 85% of its initial value, HCO<sub>ad</sub> intensity (1768 cm<sup>-1</sup>): < 50% of its initial value). In the following GC measurement, 32 min after switching the gas flow, and in later ones, no measurable formation of CH<sub>4</sub> was detected any more. At this point, the intensity of the CO<sub>ad</sub> and HCO<sub>ad</sub> related band intensities had decreased to about 78% and 22% of their initial value, respectively. The trends for CH<sub>4</sub> formation and HCO<sub>ad</sub> coverage are in complete contrast to the desorption / reaction behavior in N<sub>2</sub>, where the CH<sub>4</sub> formation rate had decreased instantaneously ( $\leq 2$  min after switching) to zero and where the formyl band had disappeared after 3–4 min. This discrepancy can be explained in the following reaction scheme. During desorption in H<sub>2</sub>, HCO<sub>ad</sub> species are continuously re-formed by reaction of already adsorbed CO<sub>ad</sub> species and H<sub>ad</sub>, where the latter is continuously replenished by adsorption from the gas phase. Apparently, the HCO<sub>ad</sub> formation rate is sufficient to largely compensate the losses in HCO<sub>ad</sub> coverage due to ongoing desorption and/or hydrogenation to CH<sub>x,ad</sub> and finally CH<sub>4,ad</sub>. During desorption in N<sub>2</sub>, in contrast, the reactive formation of HCO<sub>ad</sub>, by reaction between CO<sub>ad</sub> and H<sub>ad</sub>, is not possible and the HCO<sub>ad</sub> coverage decreases rapidly. This way, the detection limit for CH<sub>4</sub> formation is already reached within 2 min or less. Because of the much larger CO<sub>ad</sub> coverage and signal intensity as compared to HCO<sub>ad</sub>, the additional loss in the CO<sub>ad</sub> related band intensity caused by CO<sub>ad</sub> hydrogenation in H<sub>2</sub>, in addition to CO desorption, is not resolved in these (reactive) desorption experiments. The absence of CH<sub>4</sub> formation in the GC

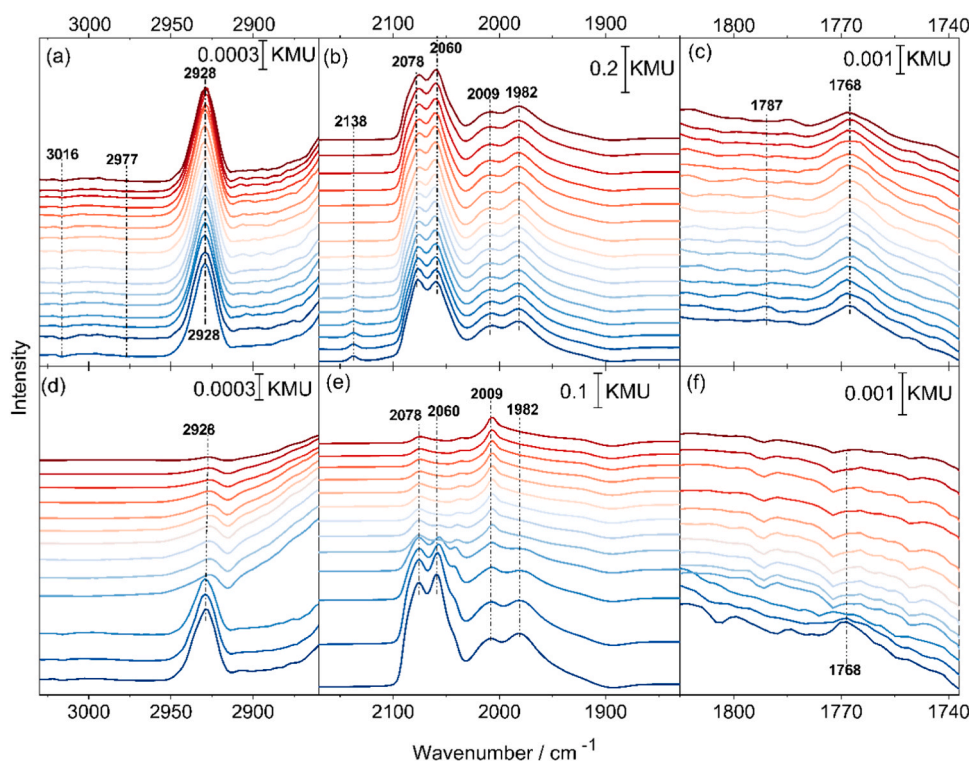


**Fig. 8.** : Series of in situ DRIFTS spectra recorded over 1000 min during isothermal desorption in  $H_2$ , after changing from ID-ref 6000 reformat gas to a flow of pure  $H_2$  at  $190^\circ C$ . Spectra recorded during the first 10 min are presented in the upper panels (a, b, c: from bottom to top: 0, 15, 30, 45, 60, 75, 90, 105, 120, 180, 240, 300, 360, 450, 540 and 600 s). Spectra recorded at extended reaction are presented in the lower panels (d, e, f: from bottom to top: 15, 30, 60, 120, 230, 290, 350, 410, 530, 650, 770, 890, 1010 min).

measurement at this stage (after 32 min), which on the first view seems to be in contrast to the ongoing presence of  $HCO_{ad}$ , is presumably due to sensitivity limitations in the GC measurements. The proposed mechanism is fully consistent with our data, although other reasons for the observed slow decay of the  $HCO_{ad}$  related signal cannot be excluded (for comparison see also ref. [14]).

The significant difference between the  $CH_4$  formation in the presence or absence of CO in the gas phase, during the isotope exchange experiment or during isothermal desorption in  $H_2$ , in combination with the small difference in initial  $CO_{ad}$  coverage in both situations (see  $CO_{ad}$  spectra in Figs. 1 and 6), seems to indicate that in the desorption experiment the reactive  $CO_{ad}$  species are rapidly depleted by desorption and/or reaction to adsorbed formyl, much faster than the total  $CO_{ad}$  intensity / coverage. Assuming that desorption and reaction of  $CO_{ad}$  follow first order kinetics with respect to  $CO_{ad}$ , this can most easily be explained in a picture where highly reactive  $CO_{ad}$  species, reactive either for hydrogenation and/or for desorption, are mainly present at high  $CO_{ad}$  coverages. In contrast,  $CO_{ad}$  species are much less active if this critical coverage is not reached any more, leading to much lower reaction / desorption rates. According to the Brønsted-Evans-Polanyi principle [82], the increase in activity at higher coverage can be explained by a destabilization of the  $CO_{ad}$  species ('destabilization of the initial state'). Hence, also from these desorption measurements we cannot decide on the relative contributions of  $CO_{ad}$  desorption and  $CO_{ad}$  hydrogenation under reaction conditions, although  $CO_{ad}$  coverage effects definitely play a role. Furthermore, we cannot distinguish whether this destabilization is a result of higher  $CO_{ad}$  –  $CO_{ad}$  repulsions (at higher  $CO_{ad}$  coverage) or due to adsorption on specific, lower energy adsorption sites. For multicarbonyl species we expect mainly the first effect to play a role.

Comparable to the situation under reaction conditions, where  $CO_{ad}$  and  $HCO_{ad}$  are close to dynamic equilibrium with the gas phase, the rates for formyl formation and formyl hydrogenation/desorption do not

differ much also in the initial phase of the desorption experiment in a  $H_2$  atmosphere, resulting in a slow variation of the  $HCO_{ad}$  coverage with time. These observations are fully consistent with our previous conclusion (see Section 3.1) that under present reaction conditions CO adsorption/desorption/hydrogenation and adsorbed formyl formation/desorption/ decomposition are essentially in equilibrium with the gas phase and with each other, and that the rate-determining step is only after these quasi-equilibria.

As main findings in this section we could demonstrate that i) the formation of adsorbed formyl species is possible in the absence of CO in the gas phase, by reaction of pre-adsorbed  $CO_{ad}$  and  $H_{ad}/H_2$ , and that ii) the formation of  $CH_{x,ad}$  species and of  $CH_4$  is possible also by reaction of adsorbed formyl species with  $H_{ad}$  in the absence of CO in the gas phase. Furthermore, the formation of adsorbed formyl species, by reaction of  $CO_{ad}$  with  $H_{ad}$ , is sufficiently fast to almost compensate losses in  $HCO_{ad}$  coverage due to decomposition or  $HCO_{ad}$  hydrogenation during desorption in  $H_2$ , resulting in an observable  $HCO_{ad}$  coverage over more than 30 min

### 3.4. $H_2/D_2$ kinetic isotope effect (KIE) – rate-determining step

Finally, we examined kinetic isotope effects (KIEs) in the CO methanation reaction for further information on the nature of the rate-determining step, comparing the rate of  $CH_4$  formation in a micro-reactor upon switching from  $^{12}CO/H_2$  to  $^{12}CO/D_2$  and back again to  $^{12}CO/H_2$  (Fig. 9a).

First, the reaction in  $^{12}CO/H_2$  was run for 490 min, until a stable rate was reached. Upon switching to  $^{12}CO/D_2$ , the rate increased abruptly from  $31.8$  to  $42.6 \mu mol_{CH_4} g_{Ru}^{-1} s^{-1}$  (after 1 min of exchange). Afterwards, the reaction rate increased slightly, but steadily for 50 min to  $44.2 \mu mol_{CH_4} g_{Ru}^{-1} s^{-1}$ , and then remained stable for 160 min in  $^{12}CO/D_2$  (Fig. 9a). The initial period reflects the increasing exchange of  $H_{ad}$  by  $D_{ad}$  species on the catalyst surface. Upon switching back from  $^{12}CO/D_2$

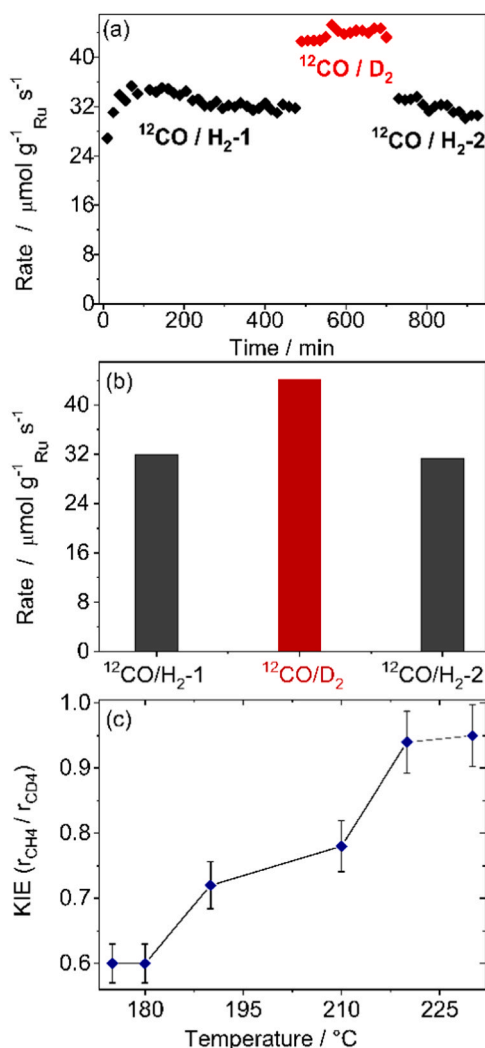


**Fig. 9.** (a) Ru mass normalized rate for  $\text{CH}_4$  formation in  $^{12}\text{CO} / \text{H}_2$  and after changing from  $^{12}\text{CO} / \text{H}_2$  ( $^{12}\text{CO} / \text{H}_2$ -1) (◆) to  $^{12}\text{CO} / \text{D}_2$  (◆) and back again to  $^{12}\text{CO} / \text{H}_2$  ( $^{12}\text{CO} / \text{H}_2$ -2) (◆) at 190  $^{\circ}\text{C}$ . (b) Steady-state rates in the different gas mixtures based on the results in (a). (c) Temperature dependence of the KIE ( $r_{\text{CH}_4} / r_{\text{CD}_4}$ ) for different reaction temperatures between 175 and 230  $^{\circ}\text{C}$ .

to  $^{12}\text{CO} / \text{H}_2$ , the reaction rate decreased initially from 44.2 to 33.3  $\mu\text{mol}_{\text{CH}_4} \text{g}_{\text{Ru}}^{-1} \text{s}^{-1}$  after 10 min and then decreased gradually for 50 min (steady-state value  $\sim 31.3 \mu\text{mol}_{\text{CH}_4} \text{g}_{\text{Ru}}^{-1} \text{s}^{-1}$ ). Hence, the steady-state rate increased by a factor of 1.4 upon the isotope exchange from  $^{12}\text{CO} / \text{H}_2$  to  $^{12}\text{CO} / \text{D}_2$ , and reversibly decreased by a similar magnitude when returning to  $^{12}\text{CO} / \text{H}_2$  (see Fig. 9b). The  $r_{\text{CH}_4} / r_{\text{CD}_4}$  ratio of about 0.71 indicates a secondary inverse KIE. Such kind of KIE has been attributed to changes in the steric environment, e.g., when a carbon bound to the H/D undergoes re-hybridization from  $\text{sp}^2$  to  $\text{sp}^3$  [83]. Consequently, breaking the  $\text{H}$  bond in the dissociative adsorption of  $\text{H}_2$  ( $\text{D}_2$ ) cannot represent the rate-determining step (RDS), and the same is true also for C-O bond breaking. Note that from the KIE results alone we are not able to distinguish whether hydrogenation of  $\text{CO}_{\text{ad}}$  or of  $\text{HCO}_{\text{ad}}$  or of later reaction intermediates represents the RDS.

Similar experiments were performed at different temperatures between 175 and 230  $^{\circ}\text{C}$ . Fig. 9c shows that increasing the reaction temperature above 180  $^{\circ}\text{C}$  results in larger KIE values for the CO methanation, until at temperatures of 220 and 230  $^{\circ}\text{C}$  ( $r_{\text{CH}_4} / r_{\text{CD}_4} = 0.95$ ) KIEs are essentially absent. Most simply, this can be understood in a model where with increasing temperature the hydrogenation step becomes increasingly faster relative to other reaction steps, until at some

point the reaction rate becomes limited by another step, e.g., by C-O bond breaking. On the other hand, for lower temperatures between 190  $^{\circ}\text{C}$  and 175  $^{\circ}\text{C}$ , the inverse KIE becomes more pronounced, reaching about 0.6 at temperatures between 180 and 175  $^{\circ}\text{C}$ . In this case, the hydrogenation step becomes more decisive for the kinetics of the methane formation rate.

As expected, a test for a similar change from  $^{12}\text{CO} / \text{H}_2$  to  $^{13}\text{CO} / \text{H}_2$  and back again to  $^{12}\text{CO} / \text{H}_2$  did not show any measurable effect.

In total, these observations indicate that under present reaction conditions and at 190  $^{\circ}\text{C}$  i) the C-H bond formation step is rate limiting for the CO methanation reaction and that ii) the relative importance of this step decreases with increasing temperature and is essentially absent at 230  $^{\circ}\text{C}$ .

### 3.5. Mechanistic pathway and rate-determining step

Based on the findings presented and discussed so far, we could clearly identify adsorbed formyl species as reaction intermediate in the dominant reaction pathway, which is formed by hydrogenation of  $\text{CO}_{\text{ad}}$ . In contrast, adsorbed formate species do not play any significant role and can essentially be excluded as reaction intermediate under present reaction conditions. Considering the rapid exchange of  $\text{CO}_{\text{ad}}$ , in particular of the multicarbonyl species, and of  $\text{HCO}_{\text{ad}}$  species in the isotope exchange measurements, which is close to that for the exchange of the gas phase, we conclude that  $\text{CO}_{\text{ad}}$  and  $\text{HCO}_{\text{ad}}$  species are essentially equilibrated with each other and with the gas phase under steady-state. This is particularly true for the multicarbonyl and formyl species, while for the other  $\text{CO}_{\text{ad}}$  species exchange is slightly slower. Most simply, this can be explained by a reaction picture where  $\text{HCO}_{\text{ad}}$  species are preferably formed by hydrogenation of more weakly adsorbed multicarbonyls, and other, more strongly adsorbed  $\text{CO}_{\text{ad}}$  species, may approximately be considered as spectator species. According to the Brønsted-Evans-Polanyi principle, the weaker bonding results in lower desorption and reaction barriers and thus in a higher hydrogenation rate constant compared to hydrogenation of the other  $\text{CO}_{\text{ad}}$  species. The much lower coverage of the adsorbed formyl species compared to  $\text{CO}_{\text{ad}}$  basically reflects the higher stability of the  $\text{CO}_{\text{ad}}$  species compared to  $\text{HCO}_{\text{ad}}$ , i.e., the higher adsorption energy of CO (and H) as compared to the sum of C-H bond formation energy, change in  $\text{C}=\text{O}$  bond energy, and HCO adsorption energy.

Such situation would be expected if the transition state for  $\text{HCO}_{\text{ad}}$  hydrogenation reflects the highest point in the free energy profile of the CO methanation reaction. In that case, in particular, if this is much higher than the levels of the preceding intermediates and transition states, the relative population of the  $\text{CO}_{\text{ad}}$  and  $\text{HCO}_{\text{ad}}$  species would be determined by the free energy difference between the two species. Exactly such kind of energy profile, with a relatively low barrier for  $\text{HCO}_{\text{ad}}$  decomposition to  $\text{H}_{\text{ad}}$  and  $\text{CO}_{\text{ad}}$ , was derived by Hibbitts et al. in their calculations for this reaction on Ru nanoparticles [29]. In this case, hydrogenation of  $\text{HCO}_{\text{ad}}$  represents the rate-determining step in the reaction under present conditions, at least in a simple picture with a single, rate-determining step (see below). In principle, such kind of equilibrium situation would also be expected for a later rate determining step. However, since we could not identify significant signals of any other subsequent reaction intermediate, hydrogenation of  $\text{HCO}_{\text{ad}}$  is favored as rate-determining step for reaction at 190  $^{\circ}\text{C}$ . The important role of the hydrogenation step is underlined also by the observation that the coverage of the  $\text{DCO}_{\text{ad}}$  intermediate is almost double as high as that of  $\text{HCO}_{\text{ad}}$ , due to differences in the zero-point energies, and by the measurements of the kinetic isotope effects. Interestingly, these latter measurements also indicated that at higher reaction temperatures the hydrogenation steps become increasingly faster relative to the other steps, and at 230  $^{\circ}\text{C}$  there is no kinetic isotope effect measurable any more for reaction in  $\text{CO} / \text{H}_2$  and  $\text{CO} / \text{CD}_4$ . Hence, at that point, hydrogenation steps are no more rate determining. It should be noted that this mechanistic pathway is only valid under present conditions (low CO:  $\text{H}_2$

ratio and  $T < 200$  °C), while at different, e.g., harsher conditions (e.g.,  $T > 250$  °C, higher pressure) or in gas mixtures containing higher CO:H<sub>2</sub> ratios, the reaction may be dominated by other mechanistic pathways such as the carbide mechanism [13,84].

The associative mechanism fits well to intuitions, as breaking of the C-O bond in CO<sub>ad</sub> with its very strong quasi-threefold bond should be a highly activated step, much more than what is expected for C-O bond breaking after partial hydrogenation of that species [28–30]. CO<sub>ad</sub> dissociation should only be competitive for substrates that lead to very strong metal-carbon and metal-oxygen bonds, which according to the Brønsted-Evans-Polanyi principle [82] should lower the activation barrier for this process by stabilizing the final state.

Our results and conclusions agree well with earlier findings on the CO methanation reaction for Ru/Al<sub>2</sub>O<sub>3</sub>, where similar type transient DRIFTS measurements also led to the conclusion of a HCO<sub>ad</sub> reaction intermediate [18]. On the other hand, for a Ru/zeolite catalyst with extremely small Ru nanoparticles of about 0.8 nm, these authors could not detect this intermediate. We speculate that this is due to a too low coverage of that species under steady-state conditions. This can result from subtle differences in the rate constants of the two reactions, adsorbed formyl formation by CO<sub>ad</sub> hydrogenation, and further hydrogenation of HCO<sub>ad</sub>, which may depend sensitively on catalyst properties such as Ru particle size and presumably also on the reaction conditions [18]. Assuming that HCO<sub>ad</sub> is also the reaction intermediate on the latter catalyst, but present only in amounts below the DRIFTS detection limit, this is a good example for the limitations in detecting reaction intermediates spectroscopically by direct observation.

Our results and conclusions are also consistent with previous results of Hibbitts et al. for the hydrogenation for CO on Ru/SiO<sub>2</sub> catalysts [29, 30]. Their DFT calculations performed on a Ru<sub>201</sub> cluster at high CO<sub>ad</sub> coverages indicated that HCO<sub>ad</sub> is formed by hydrogenation of CO<sub>ad</sub> in a quasi-equilibrated step with a low barrier for the reverse reaction, while the barrier for HCO<sub>ad</sub> hydrogenation is much higher. This agrees perfectly with our finding of a clearly measurable coverage of adsorbed formyl species and the rather fast exchange of the CO<sub>ad</sub> and HCO<sub>ad</sub> species, rapidly following the composition of the gas phase. For the next steps, their calculations favored that HCO<sub>ad</sub> is hydrogenated to adsorbed hydroxymethylene (HCOH<sub>ad</sub>). This latter step is slow, as indicated by its significantly higher barrier compared to decomposition of HCO<sub>ad</sub> into CH<sub>ad</sub> and O<sub>ad</sub>. Finally, they found that the C-O bond is broken by an essentially irreversible decomposition of the HCOH<sub>ad</sub> intermediate, leading to CH<sub>ad</sub> and OH<sub>ad</sub> [29]. Their results are consistent with ours in that i) an associative pathway via adsorbed formyl formation is favored and that ii) the calculated barrier for HCO<sub>ad</sub> decomposition to CO<sub>ad</sub> and H<sub>ad</sub> is small enough to allow quasi-equilibration between CO<sub>ad</sub> and HCO<sub>ad</sub>, while the activation barrier for HCO<sub>ad</sub> hydrogenation is much higher. It should be noted that these calculations were performed for the first steps of the Fischer-Tropsch reaction, where the composition of the reaction gas mixture is quite different (higher CO: H<sub>2</sub> ratio). The good agreement of these calculations with our experimental findings indicates that the step favoring methanation or CH<sub>x</sub> insertion occurs only later, after HCO<sub>ad</sub> hydrogenation [29,30]. For comparison, Shetty et al. reported DFT calculations on a more rough Ru(11–21) surface that also favored a hydrogen-assisted dissociation of CO<sub>ad</sub> for the first steps of the Fischer-Tropsch reaction [23].

The DFT calculations of Hibbitts et al. furthermore indicated a second pathway, via hydrogenation of CO<sub>ad</sub> to adsorbed hydroxyl-methylidyne (COH<sub>ad</sub>) [29]. This shows a similar size effective barrier, which is dominated by the first hydrogenation step. They found this pathway, however, to be inconsistent with their kinetic results. Mohan et al. concluded from a combined DFT and microkinetic study that on Ru CO<sub>ad</sub> is hydrogenated to COH<sub>ad</sub>, which then decomposes to CH<sub>ad</sub> and O<sub>ad</sub> [85]. From our data we have no evidence for a pathway involving the formation and further reaction of COH<sub>ad</sub>, e.g., by spectroscopy, although we cannot fully exclude contributions from this pathway.

Considering that in our early transient DRIFTS study on CO

methanation over a Ru/Al<sub>2</sub>O<sub>3</sub> catalyst we had identified adsorbed formyl species as intermediate and concluded on an associative mechanism study [18], metal-support interactions effects caused by the different reducibility of the supports Al<sub>2</sub>O<sub>3</sub> and TiO<sub>2</sub> are not sufficient to change the reaction pathway. A comparable reaction pathway was also concluded for CO methanation on very small Ru clusters, based on ion trap experiments, i.e., in the absence of a support, and first principle calculations [86]. These authors also observed a stabilization of H<sub>ad</sub> species by coadsorbed CO. Also for other metals such as Co [14,43] or Rh [35,36], a mechanism proceeding via the H-assisted dissociation of CO<sub>ad</sub>, via the formation of formyl species, and subsequent hydrogenation of the resulting adsorbed species, was concluded from SSITKA measurements while others discussed a direct CO dissociation pathway for these catalysts [33,87]. Overall, our conclusion of an associative (H-assisted) pathway via a formyl intermediate with C-H bond formation, most likely HCO<sub>ad</sub> hydrogenation, as rate-determining step, is fully consistent with our data and also with results of previous experimental and theoretical studies on Ru nanoparticles [29] or on supported Ru catalysts. Nevertheless, we cannot exclude contributions from a dissociative pathway, via C-O bond breaking in CO<sub>ad</sub>, which does not have intermediates with strong IR signals.

Finally, we would like to comment on the role of the rate-determining step in this reaction. As discussed above, our data clearly suggest a hydrogenation step, most likely the hydrogenation of HCO<sub>ad</sub>, as the slowest reaction step, while the preceding ones are much faster and the intermediates are essentially equilibrated. For a more detailed understanding, however, one has to keep in mind that the earlier picture of a single rate-determining step as slowest step is based on a simplified picture [79]. It is widely accepted by now that the rate-determining step is defined as the reaction step where the related transition state has the highest degree of rate control, or more simply, as the reaction step where a small change in the standard free energy of the transition state has the highest impact on the overall reaction rate [88,89]. Following this picture it may well be that CO<sub>ad</sub> hydrogenation also has some effect on the CH<sub>4</sub> formation rate, but to a lesser degree. Quantitative clarification of the role of the rate-determining step of this reaction under present reaction conditions would require, however, detailed kinetic data and calculations which are outside the scope of the present paper.

In total, our findings can confirm experimentally the reaction scheme and the reaction steps indicated in the schematic representation in Fig. 10, while details on the hydrogenation product of HCO<sub>ad</sub> and subsequent hydrogenation and C-O bond breaking steps are not accessible from these data.

As a last point we would like to mention that the present mechanistic conclusions are valid for the present reaction conditions, in particular for the idealized composition of the reaction gas with a very low CO: H<sub>2</sub> ratio, and that future work needs to extend this to more realistic compositions of the reaction gas, including higher CO concentrations and possibly also co-reactants such as CO<sub>2</sub> and H<sub>2</sub>O.

#### 4. Conclusions

Based on results of a combination of various different transient DRIFTS measurements, including the exchange of isotope labelled reactants, and measurements of the kinetic isotope effect, we could clearly demonstrate that under present reaction conditions, at low CO: H<sub>2</sub> ratios and at 190 °C, the methanation of CO on a Ru/TiO<sub>2</sub> catalyst proceeds via an associative mechanism, via the formation and further hydrogenation of an adsorbed formyl reaction intermediate. Under these conditions, the reaction is limited by C-H bond formation, most likely in the formyl hydrogenation step, leading to a quasi-equilibration of CO<sub>ad</sub> and HCO<sub>ad</sub> under steady-state conditions. The hydrogenation of HCO<sub>ad</sub> is slow enough and the energy difference between CO<sub>ad</sub> and HCO<sub>ad</sub> is small enough to result in a clearly measurable coverage of that reaction intermediate. Later rate-determining hydrogenation and C-O bond breaking steps can essentially be excluded based on the negligible

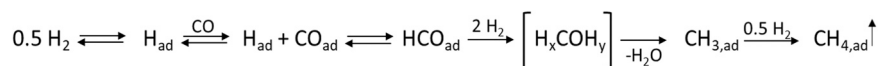


**Fig. 10.** : Schematic representation of the reaction mechanism for CO methanation on a Ru/TiO<sub>2</sub> catalyst under present reaction conditions, indicating the experimentally confirmed reaction intermediates and steps.

intensity and coverage of the related intermediates. Finally, the formation of formate intermediates and their participation in the reaction can be excluded from isotope labelling experiments, and there is also no evidence for the formation of a COH<sub>ad</sub> intermediate which had been discussed earlier.

At higher temperatures, the hydrogenation of HCO<sub>ad</sub> increasingly loses its rate-determining character and at 230 °C the reaction is limited by other steps, most likely C-O bond breaking in one of the adsorbed species resulting from HCO<sub>ad</sub> hydrogenation. While often discussed, these fundamental mechanistic aspects had not been identified by direct experimental observation on Ru catalysts so far. The study clearly demonstrates the potential of transient measurements for the clarification of the reaction mechanism in catalytic reactions.

## Funding

This research did not receive any specific grant from funding agencies in the public, commercial, or not-for-profit sector.

## CRediT authorship contribution statement

**Behm R. Jürgen:** Conceptualization, Project administration, Supervision, Writing – review & editing, Methodology. **Abdel-Mageed Ali M.:** Data curation, Formal analysis, Writing – original draft, Investigation, Methodology.

## Declaration of Competing Interest

The authors declare that they have no known competing financial interests or personal relationships that could have appeared to influence the work reported in this paper.

## Data availability

Data will be made available on request.

## Acknowledgements

We gratefully acknowledge D. Widmann for his contributions in the early phase of the experiments and also would like to thank C.T. Campbell for helpful discussions.

## Appendix A. Supporting information

Supplementary data associated with this article can be found in the online version at [doi:10.1016/j.apcatb.2024.123778](https://doi.org/10.1016/j.apcatb.2024.123778).

## References

- [1] S. Takenaka, T. Shimizu, K. Otsuka, *Int. J. Hydrog. Energy* 29 (2004) 1065.
- [2] R.M. Navarro, M.A. Pena, J.L.G. Fierro, *Chem. Rev.* 107 (2007) 3952.
- [3] G. Ercolino, M.A. Ashraf, V. Specchia, S. Specchia, *Appl. Energy* 141 (2015) 138.
- [4] C. Vogt, M. Monai, G.J. Kramer, B.M. Weckhuysen, *Nat. Catal.* 2 (2019) 188.
- [5] P. Panagiotopoulou, D.I. Kondarides, X.E. Verykios, *Appl. Catal. A* 344 (2008) 45.
- [6] P. Panagiotopoulou, D.I. Kondarides, X.E. Verykios, *J. Phys. Chem. C* 115 (2011) 1220.
- [7] C. Galletti, S. Specchia, G. Saracco, V. Specchia, *Chem. Engin. Sci.* 65 (2010) 590.
- [8] S. Eckle, Y. Denkwitz, R.J. Behm, *J. Catal.* 269 (2010) 255.
- [9] A. Chen, T. Miyao, K. Higashiyama, H. Yamashita, M. Watanabe, *Angew. Chem. Int. Ed.* 49 (2010) 9895.
- [10] A.M. Abdel-Mageed, S. Eckle, R.J. Behm, *J. Am. Chem. Soc.* 137 (2015) 8672.
- [11] A.M. Abdel-Mageed, D. Widmann, S.E. Olesen, I. Chorkendorff, J. Biskupek, R. J. Behm, *ACS Catal.* 5 (2015) 6753.
- [12] S. Chen, A.M. Abdel-Mageed, C. Gauckler, S.E. Olesen, R.J. Behm, *J. Catal.* 373 (2019) 103.
- [13] D.W. Goodman, R.D. Kelley, T.E. Madey, J.T. Yates, *J. Catal.* 63 (1980) 226.
- [14] M.A. Vasilades, N.S. Govender, A. Govender, R. Crous, D. Moodley, T. Botha, A. M. Efstathiou, *ACS Catal.* 12 (2022) 15110.
- [15] I.A. Fisher, A.T. Bell, *J. Catal.* 162 (1996) 54.
- [16] J.L.C. Fajín, J.R.B. Gomes, M.N.D.S. Cordeiro, *J. Phys. Chem. C* 119 (2015) 16537.
- [17] M.P. Andersson, F. Abild-Pedersen, I.N. Remediakis, T. Bligaard, G. Jones, J. Engbæk, O. Lytken, S. Hørch, J.H. Nielsen, J. Sehested, J.R. Rostrup-Nielsen, J. K. Nørskov, I. Chorkendorff, *J. Catal.* 255 (2008) 6.
- [18] S. Eckle, H.-G. Anfang, R.J. Behm, *J. Phys. Chem. C* 115 (2011) 1361.
- [19] M.A. Vannice, *Catal. Rev.* 14 (1976) 153.
- [20] E. Iglesia, S.C. Reyes, R.J. Madon, S.L. Soled, in: D.D. Eley, H. Pines, P.B. Weisz (Eds.), *Advances in Catalysis*, 39, Academic Press, 1993.
- [21] M.P. Andersson, T. Bligaard, A. Kustov, K.E. Larsen, J. Greeley, T. Johannessen, C. H. Christensen, J.K. Nørskov, *J. Catal.* 239 (2006) 501.
- [22] O.R. Inderwildi, S.J. Jenkins, D.A. King, *J. Phys. Chem. C* 112 (2008) 1305.
- [23] S. Shetty, A.P.J. Jansen, R.A. van Santen, *J. Am. Chem. Soc.* 131 (2009) 12874.
- [24] M. Zhuo, K.F. Tan, A. Borgna, M. Saeys, *J. Phys. Chem. C* 113 (2009) 8357.
- [25] M. Ojeda, R. Nabar, A.U. Nilekar, A. Ishikawa, M. Mavrikakis, E. Iglesia, *J. Catal.* 272 (2010) 287.
- [26] M. Ojeda, A. Li, R. Nabar, A.U. Nilekar, M. Mavrikakis, E. Iglesia, *J. Phys. Chem. C* 114 (2010) 19761.
- [27] M.R. Elahifard, M.P. Jigato, J.W. Niemantsverdriet, *ChemPhysChem* 13 (2012) 89.
- [28] B.T. Loveless, C. Buda, M. Neurock, E. Iglesia, *J. Am. Chem. Soc.* 135 (2013) 6107.
- [29] D. Hibbitts, B.T. Loveless, M. Neurock, E. Iglesia, *Angew. Chem. Int. Ed.* 52 (2013) 12273.
- [30] D. Hibbitts, E. Dybeck, T. Lawlor, M. Neurock, E. Iglesia, *J. Catal.* 337 (2016) 91.
- [31] F. Meunier, D. Reid, A. Goguet, S. Shekhtman, C. Hardacre, R. Burch, W. Deng, M. Flytzani-Stephanopoulos, *J. Catal.* 247 (2007) 277.
- [32] M. Zabilskiy, V.L. Sushkevich, D. Palagin, M.A. Newton, F. Krumeich, J.A. van Bokhoven, *Nat. Commun.* 11 (2020) 2409.
- [33] P. Biloen, J.N. Helle, F.G.A. van den Berg, W.M.H. Sachtler, *J. Catal.* 81 (1983) 450.
- [34] D.M. Stockwell, J.S. Chung, C.O. Bennett, *J. Catal.* 112 (1988) 135.
- [35] A.M. Efstathiou, C.O. Bennett, *J. Catal.* 120 (1989) 137.
- [36] A.M. Efstathiou, T. Chafik, D. Bianchi, C.O. Bennett, *J. Catal.* 147 (1994) 24.
- [37] A.M. Efstathiou, T. Chafik, D. Bianchi, C.O. Bennett, *J. Catal.* 148 (1994) 224.
- [38] M.W. Balakos, S.S.C. Chuang, G. Srinivas, *J. Catal.* 140 (1993) 281.
- [39] N. Lohitharn, J.G. Goodwin, *J. Catal.* 260 (2008) 7.
- [40] J. Yang, E.Z. Tveten, D. Chen, A. Holmen, *Langmuir* 26 (2010) 16558.
- [41] Y. Qi, J. Yang, D. Chen, A. Holmen, *Catal. Lett.* 145 (2015) 145.
- [42] D. Lorito, H. Li, A. Travert, F. Maugé, F.C. Meunier, Y. Schuurman, C. Irodatos, *Catal. Today* 299 (2018) 172.
- [43] M.A. Vasilades, C.M. Kalamaras, N.S. Govender, A. Govender, A.M. Efstathiou, *J. Catal.* 379 (2019) 60.
- [44] P. Panagiotopoulou, D.I. Kondarides, X.E. Verykios, *Appl. Catal. B* 88 (2009) 470.
- [45] A.R. Dagle, Y. Wang, G.-G. Xia, J.J. Strohm, J. Holladay, D.R. Palo, *Appl. Catal. A* 326 (2007) 213.
- [46] P. Gao, L. Zhong, L. Zhang, H. Wang, N. Zhao, W. Wei, Y. Sun, *Catal. Sci. Technol.* 5 (2015) 4365.
- [47] S. Tada, R. Kikuchi, *Catal. Sci. Technol.* 5 (2015) 3061.
- [48] C. Galletti, S. Specchia, V. Specchia, *Chem. Eng. J.* 167 (2011) 616.
- [49] S. Eckle, M. Augustin, H.-G. Anfang, R.J. Behm, *Catal. Today* 181 (2012) 40.
- [50] A.M. Abdel-Mageed, S. Eckle, H.-G. Anfang, R.J. Behm, *J. Catal.* 298 (2013) 148.
- [51] A.M. Abdel-Mageed, D. Widmann, S.E. Olesen, I. Chorkendorff, R.J. Behm, *ACS Catal.* 8 (2018) 5399.
- [52] A.M. Abdel-Mageed, D. Widmann, S. Eckle, R.J. Behm, *ChemSusChem* 8 (2015) 3869.
- [53] A.M. Abdel-Mageed, S. Eckle, R.J. Behm, *J. Catal.* 335 (2016) 79.
- [54] S. Chen, A.M. Abdel-Mageed, C. Mochizuki, T. Ishida, T. Murayama, J. Rabeah, M. Parlinska-Wojtan, A. Brückner, R.J. Behm, *ACS Catal.* 11 (2021) 9022.
- [55] P. Sabatier, *Ber. Dtsch. Chem. Ges.* 44 (1911) 1984.
- [56] A.M. Abdel-Mageed, K. Wiese, M. Parlinska-Wojtan, J. Rabeah, A. Brückner, R. J. Behm, *Appl. Catal. B* 270 (2020) 118846.
- [57] A.M. Abdel-Mageed, K. Wiese, A. Hauble, J. Bansmann, J. Rabeah, M. Parlinska-Wojtan, A. Brückner, R.J. Behm, *J. Catal.* 401 (2021) 160.
- [58] S. Cisneros, S. Chen, T. Diemant, J. Bansmann, A.M. Abdel-Mageed, M. Goepel, S. E. Olesen, E.S. Welter, M. Parlinska-Wojtan, R. Gläser, I. Chorkendorff, R.J. Behm, *Appl. Catal. B* 282 (2021), 119483-11.
- [59] A.M. Abdel-Mageed, A.Y. Klyushin, A. Knop-Gericke, R. Schlögl, R.J. Behm, *Angew. Chem. Int. Ed.* 58 (2019) 10325.
- [60] A.M. Abdel-Mageed, A. Klyushin, A. Knop-Gericke, R. Schlögl, R.J. Behm, *J. Phys. Chem. Lett.* 10 (2019) 3645.
- [61] K. Wiese, A.M. Abdel-Mageed, A. Klyushin, R.J. Behm, *Catal. Today* 336 (2019) 193.
- [62] A. Chen, X. Yu, Y. Zhou, S. Miao, Y. Li, S. Kuld, J. Sehested, J. Liu, T. Aoki, S. Hong, M.F. Camellone, S. Fabris, J. Ning, C. Jin, C. Yang, A. Nefedov, C. Wöll, Y. Wang, W. Shen, *Nat. Catal.* 2 (2019) 334.

- [63] A.M. Abdel-Mageed, B. Rungtaweeworant, S. Impeng, J. Bansmann, J. Rabeah, S. Chen, T. Häring, S. Namuangrak, K. Faungnawakij, A. Brückner, R.J. Behm, *Angew. Chem. Int. Ed.* **62** (2023) e202301920.
- [64] I.M. Hamadeh, S.A. Yeboah, K.A. Trumbull, P.R. Griffiths, *Appl. Spectrosc.* **38** (1984) 486.
- [65] J. Sirita, S. Phanichphant, F.C. Meunier, *Anal. Chem.* **79** (2007) 3912.
- [66] S.Y. Chin, C.T. Willimas, M.D. Amiridis, *J. Phys. Chem. B* **110** (2006) 871.
- [67] Y. Yan, Q. Wang, C. Jiang, Y. Yao, D. Lu, J. Zheng, Y. Dai, H. Wang, Y. Yang, *J. Catal.* **367** (2018) 194.
- [68] K. Hadjiivanov, J.-C. Lavalley, J. Lamotte, F. Maugé, J. Saint-Just, M. Che, *J. Catal.* **176** (1998) 415.
- [69] C. Mihut, C. Descorme, D. Duprez, M. Amiridis, *J. Catal.* **212** (2002) 125.
- [70] S.J. Park, X. Wang, M.R. Ball, L. Proano, Z. Wu, C.W. Jones, *Catal. Sci. Technol.* **12** (2022) 4637.
- [71] W.J. Mitchell, Y. Wang, J. Xie, W.H. Weinberg, *J. Am. Chem. Soc.* **115** (1993) 4381.
- [72] H. Yang, *Surf. Sci.* **343** (1995) 61.
- [73] H. Yang, J.L. Whitten, *Langmuir* **11** (1995) 853.
- [74] G.J. Jiang, W.B. Person, K.G. Brown, *J. Chem. Phys.* **62** (1975) 1201.
- [75] S.V. Ryazantsev, D.A. Tyurin, V.I. Feldman, *Spectrochim. Acta A* **187** (2017) 39.
- [76] R.A. MacPhail, H.L. Strauss, R.G. Snyder, C.A. Elliger, *J. Phys. Chem.* **88** (1984) 334.
- [77] G. Busca, J. Lamotte, J.-C. Lavalley, V. Lorenzelli, *J. Am. Chem. Soc.* **109** (1987) 5197.
- [78] H.M. Niederer, X.G. Wang, T. Carrington, S. Albert, S. Bauerecker, V. Boudon, M. Quack, *J. Mol. Spectrosc.* **291** (2013) 33.
- [79] M. Boudart, *Kinetics of Chemical Processes*, Butterworth-Heinemann, Boston, London, 1991.
- [80] A. Ueno, T. Onishi, K. Tamaru, *Trans. Faraday Soc.* **66** (1970) 756.
- [81] H. Pfnür, P. Feulner, D. Menzel, *J. Chem. Phys.* **79** (1983) 4613.
- [82] B. Hammer, J.K. Nørskov, *Adv. Catal.* **45** (2000) 71.
- [83] A. Streitwieser, *Molecular Orbital Theory for Organic Chemists*, John Wiley & Sons, New York, 1961.
- [84] A.T. Bell, *Catal. Rev.* **23** (1981) 203.
- [85] O. Mohan, S. Shambhawi, R. Xu, A.A. Lapkin, S.H. Mushrif, *ChemCatChem* **13** (2021) 2420.
- [86] S.M. Lang, T.M. Bernhardt, M. Krstic, V. Bonacic-Koutecky, *Angew. Chem. Int. Ed.* **53** (2014) 5467.
- [87] F. Yang, Y.M. Choi, P. Liu, J. Hrbek, J.A. Rodriguez, *J. Phys. Chem. C* **114** (2010) 17042.
- [88] C.T. Campbell, *ACS Catal.* **7** (2017) 2770.
- [89] C.T. Campbell, Z. Mao, *J. Catal.* **404** (2021) 647.